Regulation of nociceptive glutamatergic signaling by presynaptic Kv3.4 channels in the rat spinal dorsal horn

Tanziyah Muqeem[1,2], Biswarup Ghosh[1,2], Vitor Pinto[3,4], Angelo C. Lepore[1,2], Manuel Covarrubias[1,2,*]

[1]Department of Neuroscience and Vickie and Jack Farber Institute for Neuroscience, Sidney Kimmel Medical College at Thomas Jefferson University, Philadelphia PA 19107
[2]Jefferson College of Biomedical Sciences at Thomas Jefferson University, Philadelphia PA 19107
[3]Life and Health Sciences Research Institute (ICVS), School of Medicine, University of Minho, Braga, Portugal
[4]ICVS/3B's, PT Government Associate Laboratory, Braga/Guimarães, Portugal

[*]To whom correspondence should be addressed:

Manuel.Covarrubias@jefferson.edu
Bluemle Life Sciences Building
233 S 10th St
Rm 231
Philadelphia, PA 19107

Abstract

Presynaptic voltage-gated K^+ (Kv) channels in dorsal root ganglion (DRG) neurons are thought to regulate nociceptive synaptic transmission in the spinal dorsal horn. However, the Kv channel subtypes responsible for this critical role have not been identified. The Kv3.4 channel is particularly important because it is robustly expressed in DRG nociceptors, where it regulates action potential (AP) duration. Furthermore, Kv3.4 dysfunction is implicated in the pathophysiology of neuropathic pain in multiple pain models. We hypothesized that, through their ability to modulate AP repolarization, Kv3.4 channels in DRG nociceptors help regulate nociceptive synaptic transmission. To test this hypothesis, we investigated Kv3.4 immunoreactivity (IR) in the rat cervical superficial dorsal horn (sDH) in both sexes, and implemented an intact spinal cord preparation to investigate glutamatergic synaptic currents from second order neurons in the sDH under conditions that selectively inhibit the Kv3.4 current. We found presynaptic Kv3.4 IR in peptidergic and non-peptidergic nociceptive fibers of the sDH. The Kv3.4 channel is hypersensitive to 4-aminopyridine (4-AP) and tetraethylammonium (TEA). Accordingly, 50 μM 4-AP and 500 μM TEA significantly prolong the AP, slow the maximum rate of repolarization in small-diameter DRG neurons, and potentiate monosynaptic excitatory post-synaptic currents (EPSCs) in dorsal horn laminae I and II through a presynaptic mechanism. In contrast, highly specific inhibitors of BK, Kv7 and Kv1 channels are less effective modulators of the AP and have little to no effect on EPSCs. The results strongly suggest that presynaptic Kv3.4 channels are major regulators of nociceptive synaptic transmission in the spinal cord.

Keywords: spinal cord, Kv channel, synaptic transmission, pain transduction

Significance Statement

Intractable neuropathic pain can result from disease or traumatic injury, and many studies have been conducted to determine the underlying pathophysiological changes. Voltage-gated ion channels, including the K^+ channel Kv3.4, are dysregulated in multiple pain models. Kv3.4 channels are ubiquitously expressed in the dorsal root ganglion (DRG) where they are major regulators of DRG excitability. However, little is known about the ionic mechanisms that regulate nociceptive synaptic transmission at the level of the first synapse in the spinal cord, which is critical to pain transmission in both intact and pathological states. Here, we show that Kv3.4 channels have a significant impact on glutamatergic synaptic transmission in the dorsal horn, further illuminating its potential as a molecular pain therapeutic target.

Introduction

Glutamatergic synaptic transmission between primary nociceptors and secondary neurons in superficial layers of the dorsal horn is a critical step in the pain signaling pathway (Tao et al., 2005). However, our understanding of the presynaptic ion channels that regulate this process is limited (Tsantoulas and McMahon, 2014). Presynaptic voltage-gated K^+ (Kv) channels are major regulators of synaptic transmission because they have a universal ability to regulate excitability in neural tissues (Dodson and Forsythe, 2004; Bean, 2007). In particular, high voltage-activating Kv channels shape the repolarization of the AP and, therefore, determine the activation of voltage-gated Ca^{++} channels directly involved in vesicular neurotransmitter release at the nerve terminal. In the CNS, Kv3 channels are the best candidates to play this role (Rudy and McBain, 2001; Ishikawa et al., 2003; Dodson and Forsythe, 2004; Goldberg et al., 2005; Kaczmarek and Zhang, 2017; Liu et al., 2017). Recent work conclusively demonstrated that Kv3.1/3.4 heteromultimers regulate AP duration in boutons of cerebellar stellate inhibitory interneurons and, thereby, help determine evoked neurotransmitter release (Rowan et al., 2014, 2016; Rowan and Christie, 2017). However, whether a similar complex regulates nociceptive glutamatergic transmission in the spinal cord dorsal horn is not known. Also, it is important to know how cell signaling pathways associated with nociception might modulate key presynaptic Kv channels (Trimmer, 2014).

Previous work reported expression of multiple Kv channels, including Kv3.4, in adult DRG neurons (Gold et al., 1996; Rasband et al., 2001; Brooke et al., 2004a; Chien et al., 2007; Ritter et al., 2012, 2015a; Trimmer, 2014; Tsantoulas and McMahon, 2014; Liu et al., 2017). We have also determined that homomultimeric Kv3.4 channels underlie the majority of the high-voltage-activating K^+ current in small-diameter dorsal root ganglion (DRG) neurons (Ritter et al.,

2012, 2015b). Supporting this assessment, we found robust expression of Kv3.4 mRNA in these neurons, which dominates the small to negligible expression of the Kv3.1, Kv3.2 and Kv3.3 mRNAs (Ritter et al., 2012). Additionally, siRNA knockdown nearly abolishes the Kv3.4 current in small-diameter DRG neurons and prolongs the duration of the action potential (AP), helping demonstrate that Kv3.4 channels are major regulators of AP repolarization in the DRG (Ritter et al., 2012, 2015b). Moreover, Kv3.4 channels enhance their activity by undergoing switching from fast-inactivating A-type to slow-inactivating delayed rectifier-type upon phosphorylation of several serines within the channel's N-terminal inactivation domain (NTID) (Covarrubias et al., 1994; Beck et al., 1998; Antz et al., 1999; Ritter et al., 2012; Zemel et al., 2017). In small-diameter DRG neurons, this mechanism shortens the AP, strongly suggesting that Kv3.4 channel activity drives repolarization of APs carrying nociceptive signaling (Ritter et al., 2012; Liu et al., 2017). Therefore, we hypothesized that Kv3.4 channels might ultimately determine nociceptive signaling at the level of the superficial dorsal horn (sDH) by regulating AP shape and duration, which would govern Ca^{++}–dependent glutamatergic vesicular release and the resulting excitatory postsynaptic current.

To test this hypothesis, we investigated Kv3.4 immunoreactivity (IR) in the sDH, which receives Aδ and C-fiber (nociceptive fiber) projections. Then, to probe the electrophysiological impact of the Kv3.4 channel, we implemented an ex vivo preparation of an intact cervical spinal cord, a method suitable for patch-clamp recordings from superficial second order dorsal horn neurons that receive nociceptive inputs. Under conditions that stimulate Aδ and C-fibers, we tested the effects of relatively specific K^+ channel inhibitors on the magnitude of excitatory postsynaptic currents (EPSCs). Along with robust presynaptic Kv3.4 IR in the sDH, the electrophysiological results demonstrate that preferential inhibition of presynaptic Kv3.4

channels potentiates EPSCs in the sDH. Consistent with the hypothesis, inhibition of somatic Kv3.4 channels in the DRG also prolongs the AP by slowing the maximum rate of repolarization. The identification of the Kv3.4 channel as a significant player in the pain signaling pathway has implications in the pathophysiology of neuropathic pain induced by spinal cord injury and other nervous system diseases (Ritter et al., 2015a, 2015b; Zemel et al., 2017).

Materials and Methods

Spinal cord preparation

All animals were treated as approved by the IACUC of Thomas Jefferson University. Time-pregnant female Sprague–Dawley rats (Taconic Farms) were maintained in the Thomas Jefferson University Animal Facility for 1 week prior to the birth of pups. For all experiments, rat pups were killed by overdose of ketamine (380 mg/kg), xylazine (40 mg/kg), and acepromazine (0.3mg/kg) followed by decapitation. Cervical spinal cords were harvested from P9-P30 rat pups of either sex in a similar manner as described in previous studies (Pinto et al., 2008, 2010; Szucs et al., 2009). The spinal column was rapidly removed and placed in dissecting artificial cerebral spinal fluid (dACSF) consisting of (in mM): 220 Sucrose, 25 $NaHCO_3$, 11 Glucose, 2.5 KCl, 0.5 $CaCl_2$, 7 $MgCl_2$ and 1.25 NaH_2PO_4 at room temperature, and bubbled with a 95% O_2/5% CO_2 gas mixture to oxygenate and adjust pH (7.3-7.4). The spinal column was pinned down with the ventral side facing up and the ventral bony laminae were removed to expose the underlying spinal cord. The dorsal roots in the cervical region are around 1-3 mm therefore dorsal root ganglia (DRG) attached to the dorsal roots were dissected out of the bony cavity intact in order to preserve as much root as possible for stimulation. Generally, segments C5-C8 were used for all experiments. The spinal cord with attached dorsal roots and DRGs was carefully lifted out of the spinal column and the cervical spinal cord region was trimmed from the rest of the cord. The dura mater was removed and ventral roots cut from the cord to reflect the dorsal roots medially, thereby exposing a strip of gray matter on the dorsolateral side of the cord corresponding to the dorsal horn. The pia mater was gently peeled off from the region of interest in order to allow access for patch electrodes and the DRG was removed from the dorsal root. The cleaned and

trimmed cervical spinal cord was then pinned onto a beveled piece of elastomer compound eraser at an angle of ~15^{o} (Fig 3A) and transferred to an incubation chamber with oxygenated artificial cerebral spinal fluid (ACSF) consisting of (in mM): 115 NaCl, 25 $NaHCO_3$, 11 Glucose, 3 KCl, 2 $CaCl_2$, 1 $MgCl_2$, and 1 NaH_2PO_4 at room temperature until ready to transfer to the patch-clamp recording chamber. Compared to previous studies using this preparation, the use of cyanoacrylate glue was exempted in favor of small pins to keep the cord at the desired angle for illumination. Additionally, this configuration allowed us to straighten out the natural curvature of the cervical cord.

Dorsal horn neuron illumination and visualization

Neurons in the dorsal horn were illuminated using oblique infrared light-emitting diodes (LED) and visualized using a RolerA-XR camera and Q-Capture Pro7 software (Pinto et al., 2008, 2010; Szucs et al., 2009; Hachisuka et al., 2016). The LED was mounted on a small micromanipulator (Narishige) placed on the microscope headstage, and the x-y-z axes were adjusted until maximal contrast was achieved. Still images were taken using the Q-Capture Pro7 software. Neurons were selected for recording based on their location in laminae I and II of the superficial dorsal horn.

Preparation of acutely dissociated DRG neurons

P7-P28 pups were killed as mentioned for spinal cord experiments and ganglia were harvested from all accessible levels and placed into Hanks' buffered saline solution (HBSS) with 10 mM HEPES. Ganglia were dissociated by treatment with 1.5 mg/mL collagenase in HBSS/HEPES solution for 30 min followed by a 15-20 min treatment with 1 mg/mL trypsin in HBSS/HEPES solution. DRG neurons were then transferred to L-15 Leibovitz medium supplemented with 10% fetal bovine serum, 2 mM L-glutamine, 24 mM $NaHCO_3$, 38 mM glucose, and 2% penicillin-

streptomycin and mechanically dissociated with a fire polished Pasteur pipette. Neurons were plated onto poly L-ornithine coated coverslips and kept at 37^{o}C for up to 48 h.

Electrophysiology

Patch electrodes were made from Corning 7056 thin wall capillary glass (Warner Instruments) and pulled with a PIP5 micropipette puller (HEKA Instruments Inc) or a P-97 micropipette puller (Sutter Instruments). Electrodes were fire polished to have tip resistances of 1–4 MΩ. Signals were amplified using a Multiclamp 700B amplifier (Molecular Devices), low-pass filtered at 2 kHz (4-pole Bessel), digitized at 10 kHz (Digidata 1440, Molecular Devices), and stored in a computer using Clampex 10.2 (Molecular Devices). Spinal cord recordings were obtained at room temperature in oxygenated ACSF and the internal pipette solution consisted of (in mM): 150 K-gluconate, 3 KCl, 1 $MgCl_2$, 1 EGTA, 10 HEPES, pH 7.3 with KOH. All spinal cord voltage-clamp recordings were conducted at holding potentials (V_H) between -70 and -80 mV, the empirically determined reversal potential of Cl^-, in order to minimize detection of any inhibitory post-synaptic currents. In some instances, recorded neurons were labeled using an Alexa Fluor-conjugated biocytin marker (Thermo Fisher) for visualization. A suction electrode was used to stimulate the dorsal root using an A-M Systems isolated pulse stimulator, model 2100. Typically, the dorsal roots were 1-3 mm in length and stimulated with pulses in the range of 100-600 μA, duration of 1 ms, and frequency of 0.1-1 Hz. Recordings of monosynaptic EPSCs were those that had no failures upon stimulation. Only monosynaptic EPSCs were chosen for further analysis.

Action potential experiments were performed on small-diameter DRG neurons (≤25 μm) as previously reported (Ritter et al., 2012, 2015a; Zemel et al., 2017). In these experiments, the external solution consisted of (in mM): 130 NaCl, 5 KCl, 2 $CaCl_2$, 1 $MgCl_2$, and 10 HEPES

while the internal solution consisted of: 130 K-MES, 1 $CaCl_2$, 1 EGTA, 10 HEPES, 2 Mg-ATP, and 0.3 Tris-GTP. Liquid junction potential (+15.2 mV for spinal cord recordings and +15.5 mV for DRG recordings) were calculated using Clampex version 10.5 software and were corrected offline.

Drugs and toxins

All toxins and drugs were stored as concentrated stocks and added to the recording solution immediately prior to recording. Tetraethylammonium-Cl (TEA; Sigma), 4-aminopyridine (4-AP; Sigma), α-dendrotoxin (α-DTX; Alomone), iberiotoxin (IbTX; Smartox) and 6-cyano-7-nitroquinoxaline-2,3-dione (CNQX disodium salt; Alomone) were dissolved in deionized water and XE991 (Alomone) was dissolved in DMSO. For DRG experiments, a 100 mM 4-AP stock solution was made and the pH was adjusted to ~7.4 with HCl prior to use.

Immunohistochemistry

Animals were killed as previously described and transcardially perfused with 0.9% saline followed by 4% paraformaldehyde (Ritter et al., 2015a; Zemel et al., 2017). Cervical spinal cords were harvested and stored in 4% paraformaldehyde (1 day), followed by 0.1 M phosphate buffer (1 day), and finally in 30% sucrose containing phosphate buffer (>3 days). The tissue was then embedded in tissue freezing medium and 30 μm sections were cut. Sections were collected on glass slides and stored until further use.

Immunohistochemistry procedures were carried out at room temperature. The slides with the sections were washed with PBS three times (5 minutes each). Sections were then blocked with 10% normal goat serum (NGS) in PBST (PBS containing 0.2% TritonX-100) for 1 hour and then incubated with guinea pig anti-CGRP (1:1000, BMA Biomedicals), rabbit anti-Kv3.4 (1:100, Alomone) or guinea pig anti-VGLUT2 (1:2000, Millipore) overnight at room

temperature. Sections were then washed three times (5 minutes each) and incubated with goat anti-rabbit Alexa Fluor 488 (1:150, Abcam) or goat anti-guinea pig Alexa Fluor 568 (1:500, Thermo Fisher) in 5% NGS in PBST for 1 hour at room temperature. The sections were then again washed with PBS three times (5 minutes each) and coverslips were added with FluorSave reagent (Calbiochem). Finally, the slides were allowed to dry at room temperature overnight and stored at 4^{o} C. For double immunostaining of Kv3.4 and IB4, Alexa Fluor 594 conjugated isolectin GS-IB4 (2 μg/ml, Thermo Fisher) was incubated for 30 minutes after completion of overnight primary and secondary antibody treatment for Kv3.4 alone. The sections were imaged on a FluoView FV1000 confocal microscope (Olympus).

Data analysis and statistics

Data processing and analysis were conducted in Clampfit 10.5 (Molecular Devices) and Origin Pro 9.1 (OriginLab Corp). Student's paired t-test was used to evaluate differences in paired data sets. Details of the statistical analyses are provided in the corresponding figure legends and exact *p* values are generally shown on the graphs. Phase plane plots for nociceptor action potentials were obtained by plotting the 1st derivative of the AP waveform vs. the membrane potential of the AP waveform, which allows visualization of rate changes as a function of voltage. Values for means are presented as Mean ± SEM (standard error of the mean) throughout.

242

243

244

245

Results

Spinal cord Kv3.4 channels are present in presynaptic peptidergic and non-peptidergic nociceptive fibers of the sDH

To probe the functional role of the Kv3.4 channel on nociceptive spinal synaptic signaling, it is important to demonstrate presynaptic Kv3.4 expression in the sDH. We conducted immunohistochemical analyses in rat pup spinal cord to assess the expression of Kv3.4, several markers of nociceptors (CGRP and IB4) and an established marker of the excitatory presynaptic compartment (VGLUT2) (Materials and Methods). We observed Kv3.4 immunoreactivity in dorsal horn laminae I-III, where it co-localized with peptidergic calcitonin gene-related peptide (CGRP) and non-peptidergic isolectin B4 (IB4) nociceptive fibers (Fig. 1A-C, Fig. 2A-C). Additionally, Kv3.4 immunoreactivity co-localized with the presynaptic glutamatergic marker VGLUT2 (Fig. 2D). Thus, Kv3.4 channels are expressed presynaptically in sDH laminae where it co-localizes with known markers of nociceptive primary afferents.

Characterization of cervical sDH neurons in an intact spinal cord preparation

To investigate spinal nociceptive synaptic transmission under conditions that preserve the integrity of neural circuitry in the cervical spinal cord, we implemented and characterized an optimized intact preparation previously developed to study the lumbar and thoracic regions (Pinto et al., 2008, 2010; Szucs et al., 2009). The cervical spinal cord presented a few challenges because of the short roots (1-3 mm) and cervical flexure (Materials and Methods). A bipolar suction electrode applied to the selected dorsal root (C5-C8) was used for electrical stimulation and oblique LED illumination allowed visualization of sDH neurons (Materials and Methods; Fig. 3A-B). We selected spinal cord neurons based on their location in laminae I or II of the sDH, and conducted whole-cell patch-clamp recordings using standard methods as previously

described (Fig. 3C-F; Materials and Methods) (Pinto et al., 2008, 2010; Szucs et al., 2009). Upon preferential electrical stimulation of C and Aδ fibers of the dorsal root (100-600 μA, 1 ms, 0.1 Hz), these neurons displayed robust monosynaptic evoked EPSCs (eEPSCs) sensitive to CNQX (1 μM), which indicates excitatory glutamatergic synaptic transmission most likely associated with nociceptive signaling (Fig 3E; Table 1). In the absence of stimulation, and at a holding potential approximately equal to the Cl^- reversal potential (to nullify inhibitory synaptic currents), these neurons also exhibited spontaneous CNQX-sensitive EPSCs (sEPSCs) resulting from spontaneous quantal release of glutamate from C and Aδ fibers and interneurons synapsing on the nociceptive laminae of the sDH (Fig. 3F). Correspondingly, under current-clamp conditions and following stimulation of the dorsal roots, we observed sub- and supra-threshold EPSPs (Fig. 4A-B). Further supporting the healthy quality of the spinal cord preparation, the selected neurons also exhibited robust passive and active membrane parameters (Fig. 4C-D; Table 2).

Evoked EPSCs in the sDH are potentiated by TEA and 4-AP but not by antagonists of BK, Kv7, and Kv1 channels

Following the demonstration of Kv3.4 channel expression in presynaptic nerve terminals of the spinal cord dorsal horn and physiological validation of the intact spinal cord preparation, we set out to determine whether this Kv channel is a regulator of synaptic transmission in the sDH. Kv3 channels are hypersensitive to low, submillimolar concentrations of the well-known K^+ channel blockers, 4-AP and TEA (Schroter et al., 1991; Vega-Saenz de Miera et al., 1992). To test the effects of these inhibitors on synaptic transmission, we held the membrane potential of the spinal cord neuron at -70 mV (~E_{Cl}) and recorded eEPSCs upon strong stimulation of the dorsal root (100-600 μA) to excite high-threshold nociceptive fibers (C and Aδ). Under these conditions,

292 the recorded eEPSC results from activation of spinal cord glutamatergic AMPA receptors (Fig.
293 3). Exposure to either 50 μM 4-AP or 500 μM TEA similarly potentiated the average peak of the
294 eEPSCs by 47.14 ± 18.69% and 20.71 ± 8.19%, respectively (Fig. 5A-B). These results suggest
295 that, through inhibition of presynaptic C/Aδ fiber K^+ channels, the presynaptic AP is prolonged
296 and, consequently, vesicular Ca^{++}–dependent glutamatergic release is enhanced.

297 However, this result alone cannot rule out possible contributions of other K^+ channels
298 that are also significantly sensitive to TEA and/or 4-AP, such as Kv1, Kv7, and big-conductance
299 Ca^{++}–activated K^+ (BK) channels (Dodson and Forsythe, 2004). Expression of these K^+ channels
300 has also been reported in putative DRG nociceptors (Everill et al., 1998; Scholz et al., 1998;
301 Rasband et al., 2001; Beekwilder et al., 2003; Zhang et al., 2003, 2010; Chi and Nicol, 2007;
302 Rose et al., 2011; Zheng et al., 2013; Martinez-Espinosa et al., 2015; Liu et al., 2017). To rule
303 out whether these K^+ channels were contributing to the observed TEA and 4-AP effects, we
304 tested α-DTX, XE991, and IbTX which are highly selective antagonists of Kv1.1/1.2/1.6, Kv7
305 and BK channels, respectively. Upon exposing spinal cords to these antagonists, we observed no
306 effect on the average peak of the eEPSCs, which is in contrast to the potentiating effects of TEA
307 and 4-AP (Fig. 6A-C). Also, α-DTX, XE991 and IbTX have little to no effect on jitter and rise
308 time of the eEPSCs (Table 3). Given the differential effects of TEA and 4-AP against the other
309 more specific K^+ channel antagonists, we can conclude that inhibition of a Kv3-type channel is
310 most likely responsible for the associated potentiation of the eEPSCs. Furthermore, Kv3.4 is the
311 top candidate. Besides its presynaptic expression in nociceptive afferents of the sDH (Fig. 1-2),
312 we have previously reported strong evidence demonstrating that Kv3.4 is the dominant Kv3
313 isoform in putative DRG nociceptors from rat pups (Ritter et al., 2012, 2015a, 2015b).

314 *TEA and 4-AP act presynaptically to potentiate the eEPSC*

The results so far are consistent with a presynaptic role of the Kv3.4 channel. However, the average peak eEPSC resulting from consecutive stimulations might include both monosynaptic and polysynaptic responses. Confirming that low concentrations of TEA and 4-AP potentiate monosynaptic eEPSCs would add strong support to a presynaptic DRG mechanism involving regulation of the AP by Kv3.4. Thus, from each stimulation run (a family of traces), we isolated consistent stable EPSC peaks (no failures) in each individual trace by-eye, segments which oftentimes coincided with the lowest variance around the peak (Fig. 7). Both methods consistently revealed similar monosynaptic peaks in individual traces, which were generally potentiated by low concentrations of TEA and 4-AP (Fig. 8A-B). By contrast, IbTX, α-DTX and XE991 had little to no effect on monosynaptic eEPSC peaks (Fig. 8C-E).

To test the presynaptic mechanism further, we also investigated the effects of the K^+ channel antagonists on the paired pulse ratio (PPR) and the amplitude of spontaneous EPSCs (sEPSC). A change in the PPR demonstrates a presynaptic effect tied to vesicle depletion inducing synaptic depression (PPR=P2/P1<1) or presynaptic Ca^{2+} accumulation associated with synaptic facilitation (PPR>1) (Fioravante and Regehr, 2011). In contrast, no PPR change would be more consistent with a postsynaptic effect that impacts paired responses equally. Generally, we found that the PPR was <1 under control conditions, indicating synaptic depression. In the presence of 4-AP and TEA, the PPR was consistently decreased further (0.79 ± 0.23 to 0.58 ± 0.24 for 4-AP, 0.69 ± 0.11 to 0.48 ± 0.11 for TEA), which suggests exacerbated vesicle depletion resulting from a presynaptic effect of the inhibitors (Fig. 9A-B).

Desensitization of postsynaptic AMPA receptors could have contributed to the observed synaptic depression (Kirischuk et al., 2002; Chen et al., 2004; Christie et al., 2010). Thus, to directly assess a possible postsynaptic phenomenon, we examined the effect of TEA on the

amplitude of sEPSCs. The origin of the sEPSCs includes vesicle release from primary DRG nociceptive afferents and spinal interneurons. To isolate the sEPSCs mainly mediated by AMPA receptor channels, we recorded the spontaneous activity at E_{Cl} (-70 mV), as done previously (Fig. 3). We observed significant spontaneous activity, which allowed robust measurements of sEPSC peak amplitudes before and after exposure to 500 μM TEA (>400 events; Fig. 10A). In three independent paired experiments, we found that the normalized amplitude histograms of the sEPSCs recorded before and after exposure to TEA were indistinguishable (Fig. 10B-C). These results ruled out a postsynaptic action of TEA, which could have been responsible for the TEA-dependent potentiation of the eEPSCs. Additionally, there was no change in the frequency of events before and after exposure to 500 μM TEA (6.22 ± 2.59 events/sec and 6.54 ± 3.37 events/sec, before and after TEA, respectively; estimates derived from data presented in Fig 10), demonstrating that TEA did not impact the level of spontaneous activity, a proxy measurement for presynaptic resting membrane potential. Based on the evidence provided by three independent experiments (monosynaptic potentiation, enhanced synaptic depression and lack of effect on sEPSC amplitude and frequency), we conclude that submillimolar 4-AP and TEA potentiate glutamatergic synaptic transmission at a presynaptic level thorough the inhibition of Kv3.4 channels in DRG neurons.

The DRG action potential is consistently modulated by the Kv channel inhibitors TEA and 4-AP

If presynaptic potentiation of the eEPSC results from prolonging the presynaptic AP upon inhibition of the Kv3.4 current in DRG neurons, we expected broadening of the somatic AP by submillimolar TEA and 4-AP and little and inconsistent effects of IbTX, α-DTX, and XE991 on somatic AP duration. This hypothesis, however, assumes that the somatic and presynaptic APs are shaped by a similar ensemble of ion channels and, therefore, similarly regulated by Kv3.4.

To test these ideas, we recorded somatic APs from acutely dissociated DRG neurons before and after the exposure to the selected K^+ channel inhibitors at the same concentrations used in the spinal cord recordings (Fig. 11; Table 4). Whereas TEA and 4-AP consistently broadened the AP (APD_{50} and APD_{90}; p = 4.99E-4 – 0.042) and slowed the maximum rate of repolarization (p = 6.99E-4 – 0.037), the effects of IbTX on these properties were inconsistent, albeit it marginally prolonged the APD_{50} (p = 0.043). By contrast, XE991 and α-DTX did not affect the AP waveform (Fig 11; Table 4). Overall, these results are consistent with a major direct role of Kv3.4 on the repolarization of the AP in DRG neurons, which secondarily regulates evoked Ca^{++}-dependent glutamatergic neurotransmission in the sDH of the spinal cord. The inconsistent results with IbTX, suggest heterogeneity and quantitative differences in the relative contributions of Kv3.4 and BK channels to AP repolarization in the soma and nerve terminals of putative nociceptors.

Discussion

The Kv3.4 channel is a major regulator of AP repolarization in small-diameter nociceptors in the DRG. Here, we asked whether this regulation actually impacts nociceptive signaling in the spinal cord. Consistent with a presynaptic localization, we found that Kv3.4 is expressed in excitatory presynaptic terminals in nociceptive afferents of the sDH, where it co-localizes with key molecular markers of the pain pathway (CGRP, IB4 and VGLUT2). Using an ex vivo preparation of the cervical spinal cord and several K^+ channel inhibitors, we demonstrate that submillimolar concentrations of 4-AP and TEA potentiate monosynaptic glutamatergic eEPSCs, suggesting that inhibition of the presynaptic 4-AP/TEA-hypersensitive Kv3.4 is responsible for this potentiation. Strengthening this conclusion, these inhibitors also decreased the PPR but did not affect the amplitude and frequency of sEPSCs. By contrast, specific inhibition of other DRG K^+ channels that also exhibit hypersensitivities to 4-AP and/or TEA did not affect the eEPSC. Further supporting a direct relationship between Kv3.4-dependent regulation of AP duration in the DRG and the eEPSC peak in the sDH, submillimolar TEA and 4-AP prolong the presynaptic AP, whereas other specific K^+ channel inhibitors induce little and inconsistent effects on the AP waveform.

Optimization of the ex vivo cervical spinal cord patch-clamping technique

Over the last decade, several studies have used intact organ spinal cord preparations to study electrophysiological and morphological parameters as well as local circuitry (Pinto et al., 2008, 2010; Szucs et al., 2009; Hachisuka et al., 2016). Compared to traditional slices, this technique has many advantages, including less damage to the spinal cord, which is especially important toward understanding the complex circuitry of the dorsal horn (Peirs and Seal, 2016). However, this technique has thus far been mainly applied to the lumbar and thoracic regions of the spinal

cord. The cervical spinal cord is important not only from a physiological perspective, but also from a relevant pathological viewpoint since the cervical region is the most common location of spinal cord injuries in humans. Thus, we focused on optimizing this preparation to expand the application and relevance of the ex vivo spinal cord technique. By minimizing the pronounced flexure of the cervical region and ensuring the viability of short dorsal roots, we obtained a robust and reliable new preparation suitable for intact spinal cord patch clamping experiments.

The presynaptic Kv3.4 channel regulates glutamatergic signaling in the superficial dorsal horn

Consistent with previous reports (Brooke et al., 2004a; Chien et al., 2007), we observed Kv3.4 expression in the neuropil of the sDH, where it co-localizes with markers of nociceptive fibers, CGRP and IB4. Additionally, our new results show that Kv3.4 found in the sDH is expressed presynaptically in glutamatergic axonal terminals, as determined by its co-localization with VGLUT2. Thus, Kv3.4 is ideally present in the terminal axonal compartment to regulate nociceptive synaptic transmission through its ability to shape AP repolarization.

Generally, presynaptic Kv channels help tune synaptic transmission by regulating the spiking properties of neurons (Dodson and Forsythe, 2004; Kaczmarek and Zhang, 2017). This information coupled with previous work demonstrating that Kv3 channels are the primary regulators of AP repolarization in the CNS and that Kv3.4 is the dominant Kv3 channel in DRG neurons, suggests that this ion channel might play a significant role as a regulator of nociceptive synaptic activity at the level of the first synapse in the pain pathway (Goldberg et al., 2005; Ritter et al., 2012; Rowan et al., 2014, 2016; Liu et al., 2017; Rowan and Christie, 2017). New data described here strongly support this hypothesis by demonstrating that a Kv channel hypersensitive to 4-AP and TEA, such as Kv3.4, regulates AP repolarization rate and duration in nociceptors and, consequently, the amplitude of the eEPSC in the sDH.

Since the Kv3.4 channel's main role is to help repolarize the AP in small-diameter DRG neurons, its inhibition would prolong the AP that ultimately reaches the nerve terminal of putative nociceptors. Thus, if the AP evoked by electrical stimulation of the dorsal root is prolonged following inhibition of the Kv3.4 channel by either TEA or 4-AP, activation of voltage-gated Ca^{++} channels and the resulting Ca^{++} entry into the nerve terminal are increased. Consequently, the probability of Ca^{++}-dependent vesicular glutamate release increases and the ensuing eEPSC is potentiated, which is in line with accepted theories of quantal neurotransmission (Katz and Miledi, 1967; Mulkey and Zucker, 1991; Llinás et al., 1992; Borst et al., 1995; Bollmann and Sakmann, 2005). The results of this work are reminiscent of the role that presynaptic Kv3.4 might play at the mouse neuromuscular junction, where inhibition of this ion channel potentiates the endplate potential (Brooke et al., 2004b). Also, the interpretation of our results gains additional support from the pattern of differential effects that K^+ channel inhibitors have on the AP waveform in the DRG, which generally mirrors the effects on the eEPSC in the sDH. In particular, however, there are interesting differences possibly reflecting quantitatively different contributions of distinct K^+ channels to AP repolarization in the soma and the nerve terminal. For instance, it appears that IbTX is capable of prolonging the AP by mainly increasing the APD_{50}, but it has no consistent effect on the eEPSC. By contrast, submillimolar 4-AP and TEA consistently lengthen the APD_{50} and APD_{90}, and accordingly potentiate the monosynaptic eEPSC. The DRG AP results are consistent with previous studies (Li et al., 2007; Zhang et al., 2010; Liu et al., 2017).

To establish that the mechanism discussed above most likely involves presynaptic regulation by Kv3.4, submillimolar TEA and 4-AP also enhanced synaptic depression by decreasing the PPR. This is likely the result of increased vesicle depletion. Moreover, we found

443 no evidence of a postsynaptic contribution because the amplitude of spontaneous EPSCs was not
444 affected by submillimolar TEA. Also, TEA had no effect on the spontaneous EPSC frequency,
445 which, under the conditions of our experiments, might originate from spontaneous release and
446 evoked release resulting from spontaneous depolarizations originating in the DRG and spinal
447 interneurons. Thus, TEA-hypersensitive K^+ channels are not regulating resting membrane
448 potential (Table 4) and spontaneous spiking, which is consistent with the interpretation of our
449 results. Kv3.4 is a high voltage-activating A-type Kv channel that is best suited to shape AP
450 repolarization, as established by recent work from us and others (Ritter et al., 2012; Rowan et al.,
451 2014, 2016; Liu et al., 2017; Rowan and Christie, 2017).

452 *The role of other K^+ channels expressed in the DRG*

453 The DRG expresses multiple K^+ channels exhibiting differential cellular and subcellular
454 distributions in heterogeneous populations of primary sensory neurons and, moreover, they share
455 major differences in terms of their gating properties and mechanisms of modulation (Gold et al.,
456 1996; Safronov et al., 1996; Rasband et al., 2001; Zhang et al., 2003, 2010; Chi and Nicol, 2007;
457 Chien et al., 2007; Phuket and Covarrubias, 2009; Duan et al., 2012; Zheng et al., 2013). Thus,
458 they play a myriad of roles along the peripheral sensory pathway, regulating resting membrane
459 potential and AP properties (shape, repolarization rate, propagation, latency to first spike,
460 interspike interval, afterhyperpolarization, etc.). By using a battery of specific K^+ channel
461 antagonists (α-DTX, XE991, IbTX) against DRG K^+ channels sharing sensitivities to
462 submillimolar concentrations of TEA and/or 4-AP, we ruled out major possible contributions of
463 several DRG K^+ channels (Kv1.1, Kv1.2, Kv1.6, Kv7 and BK channels) to nociceptive synaptic
464 transmission in the sDH. Although BDS-I is thought to be a specific Kv3.4 peptide inhibitor, we
465 did not use it in these experiments, because it also potentiates Nav1.7 with high potency, a

critical voltage-gated Na^+ channel expressed in primary sensory neurons (Diochot et al., 1998; Liu et al., 2012). It is also unlikely that DRG Kv1.4 and Kv4 channels contribute presynaptically to synaptic transmission in the sDH because they are low voltage-activating, highly resistant to TEA, and only modestly sensitive to 4-AP. Furthermore, the expression of Kv4.1 and Kv4.3 is limited to the soma of rat DRG neurons (Gold et al., 1996; Chien et al., 2007; Phuket and Covarrubias, 2009; Yunoki et al., 2014). Additionally, other channels, such as Kv2 and Slack channels, are also expressed in the DRG but are unlikely to be candidates because they are relatively insensitive to TEA and 4-AP (Patel et al., 1997; Bocksteins et al., 2009; Lu et al., 2015). Overall, these results strongly suggest that Kv3.4, the most likely target of submillimolar TEA and 4-AP, is a major presynaptic regulator of excitatory neurotransmission from glutamatergic C- and Aδ-fibers in the sDH.

Implications and Perspective

Previous work and the new results presented here collectively constitute compelling evidence for the presynaptic role of the Kv3.4 channel as a significant regulator of glutamatergic synaptic signaling in the spinal cord nociceptive pathway. These findings help explain how SCI-induced dysfunction of the Kv3.4 channel in primary nociceptors can lead to intractable neuropathic pain. Thus, the Kv3.4 channel is an attractive target that might help develop more effective interventions to alleviate persistent pain induced by SCI and other nervous system diseases associated with pathological pain. Any manipulations that increase Kv3.4 activity in the DRG might have beneficial analgesic effects.

Acknowledgments: This work was supported by the Vickie and Jack Farber Foundation (M.C.), the Dean's Transformational Science Award (M.C.), the National Institutes of Health (Grant

NS079855 to M.C. and Grant NS079702 to A.C.L.), the Dubbs Fellowship Fund (T.M.), Sigma Xi GIAR G20141015648241 (T.M.), Autifony Therapeutics, Ltd. (M.C.) and the Luso-American Development Foundation (V.P.). We thank Drs. Matthew Dalva, Melanie Elliott, Ethan Goldberg, David Ritter, Benjamin Zemel and members of the Covarrubias lab for helpful comments and feedback on previous versions of this manuscript, and the Dalva Lab for sharing reagents. Additionally, we thank Dr. Bruce Bean for providing helpful tips regarding the effects of Kv channel inhibitors on the action potential in the DRG. The authors declare no competing financial interests.

References

Antz C, Bauer T, Kalbacher H, Frank R, Covarrubias M, Robert H, Ruppersberg JP, Kalbitzer HR, Ruppersberg JP, Baukrowitz T, Fakler B (1999) Control of K^+ channel gating by protein phosphorylation: structural switches of the inactivation gate. Nat Struct Biol 6:146–150.

Bean BP (2007) The action potential in mammalian central neurons. Nat Rev Neurosci 8:451–465.

Beck EJ, Sorensen RG, Slater SJ, Covarrubias M (1998) Interactions between multiple phosphorylation sites in the inactivation particle of a K^+ channel. Insights into the molecular mechanism of protein kinase C action. J Gen Physiol 112:71–84.

Beekwilder JP, O'Leary ME, Broek LP Van Den, Kempen GTH Van, Ypey DL, Berg RJ Van Den (2003) Kv1.1 channels of dorsal root ganglion neurons are inhibited by n-butyl-p-aminobenzoate, a promising anesthetic for the treatment of chronic pain. Pharmacology 304:531–538.

Bocksteins E, Raes AL, Vijver G Van De, Bruyns T, Bogaert P-P Van, Snyders DJ (2009) Kv2.1 and silent Kv subunits underlie the delayed rectifier K+ current in cultured small mouse DRG neurons. Am J Physiol Cell Physiol 296:1271–1278.

Bollmann JH, Sakmann B (2005) Control of synaptic strength and timing by the release-site Ca^{2+} signal. Nat Neurosci 8:426–434.

Borst JG, Helmchen F, Sakmann B (1995) Pre- and postsynaptic whole-cell recordings in the

542 medial nucleus of the trapezoid body of the rat. J Physiol 489:825–840.

543 Brooke RE, Atkinson L, Batten TFC, Deuchars SA, Deuchars J (2004a) Association of
544 potassium channel Kv3.4 subunits with pre- and post-synaptic structures in brainstem and
545 spinal cord. Neuroscience 126:1001–1010.

546 Brooke RE, Moores TS, Morris NP, Parson SH, Deuchars J (2004b) Kv3 voltage-gated
547 potassium channels regulate neurotransmitter release from mouse motor nerve terminals.
548 Eur J Neurosci 20:3313–3321.

549 Chen G, Harata NC, Tsien RW (2004) Paired-pulse depression of unitary quantal amplitude at
550 single hippocampal synapses. Proc Natl Acad Sci U S A 101:1063–1068.

551 Chi XX, Nicol GD (2007) Manipulation of the potassium channel Kv1.1 and its effect on
552 neuronal excitability in rat sensory neurons. J Neurophysiol 98:2683–2692.

553 Chien L-Y, Cheng J-K, Chu D, Cheng C-F, Tsaur M-L (2007) Reduced Expression of A-Type
554 Potassium Channels in Primary Sensory Neurons Induces Mechanical Hypersensitivity. J
555 Neurosci 27:9855–9865.

556 Christie LA, Russell TA, Xu J, Wood L, Shepherd GMG, Contractor A (2010) AMPA receptor
557 desensitization mutation results in severe developmental phenotypes and early postnatal
558 lethality. Proc Natl Acad Sci U S A 107:9412–9417.

559 Covarrubias M, Wei A, Salkoff L, Vyas TB (1994) Elimination of rapid potassium channel
560 inactivation by phosphorylation of the inactivation gate. Neuron 13:1403–1412.

561 Diochot S, Schweitz H, Béress L, Lazdunski M (1998) Sea anemone peptides with a specific
562 blocking activity against the fast inactivating potassium channel Kv3.4. J Biol Chem
563 273:6744–6749.

564 Dodson PD, Forsythe ID (2004) Presynaptic K+ channels: Electrifying regulators of synaptic
565 terminal excitability. Trends Neurosci 27:210–217.

566 Duan K-Z, Xu Q, Zhang X-M, Zhao Z-Q, Mei Y-A, Zhang Y-Q (2012) Targeting A-type K^+
567 channels in primary sensory neurons for bone cancer pain in a rat model. Pain 153:562–574.

568 Everill B, Rizzo MA, Kocsis JD (1998) Morphologically Identified Cutaneous Afferent DRG
569 Neurons Express Three Different Potassium Currents in Varying Proportions. J
570 Neurophysiol 79:1814–1824.

571 Fioravante D, Regehr WG (2011) Short-term forms of presynaptic plasticity. Curr Opin
572 Neurobiol 21:269–274.

573 Gold MS, Shuster MJ, Levine JD (1996) Characterization of six voltage-gated K^+ currents in
574 adult rat sensory neurons. J Neurophysiol 75:2629–2646.

575 Goldberg EM, Watanabe S, Chang SY, Joho RH, Huang ZJ, Leonard CS, Rudy B (2005)
576 Specific Functions of Synaptically Localized Potassium Channels in Synaptic Transmission
577 at the Neocortical GABAergic Fast-Spiking Cell Synapse. J Neurosci 25:5230–5235.

578 Hachisuka J, Baumbauer KM, Omori Y, Snyder LM, Koerber HR, Ross SE (2016) Semi-intact
579 ex vivo approach to investigate spinal somatosensory circuits. Elife 5:1–19.

580 Ishikawa T, Nakamura Y, Saitoh N, Li W-B, Iwasaki S, Takahashi T (2003) Distinct roles of
581 Kv1 and Kv3 potassium channels at the calyx of Held presynaptic terminal. J Neurosci
582 23:10445–10453.

583 Kaczmarek LK, Zhang Y (2017) Kv3 Channels: Enablers of Rapid Firing, Neurotransmitter
584 Release, and Neuronal Endurance. Physiol Rev 97:1431–1468.

585 Katz B, Miledi R (1967) The timing of calcium action during neuromuscular transmission. J

586 Physiol 189:535–544.

587 Kirischuk S, Clements JD, Grantyn R (2002) Presynaptic and postsynaptic mechanisms underlie
588 paired pulse depression at single GABAergic boutons in rat collicular cultures. J Physiol
589 543:99–116.

590 Li W, Gao S-B, Lv C-X, Wu Y, Guo Z-H, Ding J-P, Xu T (2007) Characterization of voltage-
591 and Ca^{2+}-activated K+ channels in rat dorsal root ganglion neurons. J Cell Physiol 212:348–
592 357.

593 Liu P, Blair NT, Bean BP (2017) Action potential broadening in capsaicin-sensitive DRG
594 neurons from frequency-dependent reduction of Kv3 current. J Neurosci:1703–1717.

595 Liu P, Jo S, Bean BP (2012) Modulation of neuronal sodium channels by the sea anemone
596 peptide BDS-I. J Neurophysiol 107:3155–3167.

597 Llinás R, Sugimori M, Silver RB (1992) Microdomains of high calcium concentration in a
598 presynaptic terminal. Science (80-) 256:677–679.

599 Lu R, Bausch AE, Kallenborn-Gerhardt W, Stoetzer C, Debruin N, Ruth P, Geisslinger G,
600 Leffler A, Lukowski R, Schmidtko A (2015) Slack Channels Expressed in Sensory Neurons
601 Control Neuropathic Pain in Mice. J Neurosci 35:1125–1135.

602 Martinez-Espinosa PL, Wu J, Yang C, Gonzalez-Perez V, Zhou H, Liang H, Xia XM, Lingle CJ
603 (2015) Knockout of Slo2.2 enhances itch, abolishes KNa current, and increases action
604 potential firing frequency in DRG neurons. Elife 4:1–27.

605 Mulkey RM, Zucker RS (1991) Action potentials must admit calcium to evoke transmitter
606 release. Nature 350:153–155.

607 Patel AJ, Lazdunski M, Honoré E (1997) Kv2.1/Kv9.3, a novel ATP-dependent delayed-rectifier

608 K+ channel in oxygen-sensitive pulmonary artery myocytes. EMBO J 16:6615–6625.

609 Peirs C, Seal RP (2016) Neural circuits for pain: Recent advances and current views. Science
610 (80-) 354:578–584.

611 Phuket TR, Covarrubias M (2009) Kv4 channels underlie the subthreshold-operating A-type K^+-
612 current in nociceptive dorsal root ganglion neurons. Front Mol Neurosci 2:1–14.

613 Pinto V, Szûcs P, Derkach VA, Safronov B V (2008) Monosynaptic convergence of C- and
614 Adelta-afferent fibres from different segmental dorsal roots on to single substantia
615 gelatinosa neurones in the rat spinal cord. J Physiol 586:4165–4177.

616 Pinto V, Szucs P, Lima D, Safronov B V (2010) Multisegmental Adelta- and C-fiber input to
617 neurons in lamina I and the lateral spinal nucleus. J Neurosci 30:2384–2395.

618 Rasband MN, Park EW, Vanderah TW, Lai J, Porreca F, Trimmer JS (2001) Distinct potassium
619 channels on pain-sensing neurons. Proc Natl Acad Sci U S A 98:13373–13378.

620 Ritter DM, Ho C, O'Leary ME, Covarrubias M (2012) Modulation of Kv3.4 channel N-type
621 inactivation by protein kinase C shapes the action potential in dorsal root ganglion neurons.
622 J Physiol 590:145–161.

623 Ritter DM, Zemel BM, Hala TJ, O'Leary ME, Lepore AC, Covarrubias M (2015a)
624 Dysregulation of Kv3.4 channels in dorsal root ganglia following spinal cord injury. J
625 Neurosci 35:1260–1273.

626 Ritter DM, Zemel BM, Lepore AC, Covarrubias M (2015b) Kv3.4 channel function and
627 dysfunction in nociceptors. Channels 9:209–217.

628 Rose K, Ooi L, Dalle C, Robertson B, Wood IC, Gamper N (2011) Transcriptional repression of
629 the M channel subunit Kv7.2 in chronic nerve injury. Pain 152:742–754.

630 Rowan MJM, Christie JM (2017) Rapid State-Dependent Alteration in Kv3 Channel Availability
631 Drives Flexible Synaptic Signaling Dependent on Somatic Subthreshold Depolarization.
632 Cell Rep 18:2018–2029.

633 Rowan MJM, DelCanto G, Yu JJ, Kamasawa N, Christie JM (2016) Synapse-Level
634 Determination of Action Potential Duration by K+ Channel Clustering in Axons. Neuron
635 91:1–14.

636 Rowan MJM, Tranquil E, Christie JM (2014) Distinct Kv channel subtypes contribute to
637 differences in spike signaling properties in the axon initial segment and presynaptic boutons
638 of cerebellar interneurons. J Neurosci 34:6611–6623.

639 Rudy B, McBain CJ (2001) Kv3 channels: Voltage-gated K^+ channels designed for high-
640 frequency repetitive firing. Trends Neurosci 24:517–526.

641 Safronov B V, Bischoff U, Vogel W (1996) Single voltage-gated K^+ channels and their functions
642 in small dorsal root ganglion neurones of rat. J Physiol 493:393–408.

643 Scholz A, Gruss M, Vogel W (1998) Properties and functions of calcium-activated K^+ channels
644 in small neurones of rat dorsal root ganglion studied in a thin slice preparation. J Physiol
645 513:55–69.

646 Schroter K-H, Ruppersberg JP, Wunder F, Rettig J, Stocker M, Pongs O (1991) Cloning and
647 functional expression of a TEA-sensitive A-type potassium channel from rat brain. FEBS
648 278:211–216.

649 Szucs P, Pinto V, Safronov B V. (2009) Advanced technique of infrared LED imaging of
650 unstained cells and intracellular structures in isolated spinal cord, brainstem, ganglia and
651 cerebellum. J Neurosci Methods 177:369–380.

652 Tao Y-X, Gu J, Stephens RL (2005) Role of Spinal Cord Glutamate Transporter during Normal
653 Sensory Transmission and Pathological Pain States. Mol Pain 1:1744-8069-1–30.

654 Trimmer JS (2014) Ion Channels and Pain: Important Steps Towards Validating a New
655 Therapeutic Target for Neuropathic Pain. Exp Neurol 254:190–194.

656 Tsantoulas C, McMahon SB (2014) Opening paths to novel analgesics: The role of potassium
657 channels in chronic pain. Trends Neurosci 37:146–158.

658 Vega-Saenz de Miera E, Moreno H, Fruhling D, Kentros C, Rudy B (1992) Cloning of ShIII
659 (Shaw-like) cDNAs encoding a novel high-voltage-activating, TEA-sensitive, type-A K^+
660 channel. Proc Biol Sci 248:9–18.

661 Yunoki T, Takimoto K, Kita K, Funahashi Y, Takahashi R, Matsuyoshi H, Naito S, Yoshimura
662 N (2014) Differential contribution of Kv4-containing channels to A-type, voltage-gated
663 potassium currents in somatic and visceral dorsal root ganglion neurons. J Neurophysiol
664 112:2492–2504.

665 Zemel BM, Muqeem T, Brown E V, Goulao M, Urban MW, Tymanskyj SR, Lepore AC,
666 Covarrubias M (2017) Calcineurin Dysregulation Underlies Spinal Cord Injury-Induced K^+
667 Channel Dysfunction in DRG Neurons. J Neurosci 37:8256–8272.

668 Zhang X-L, Mok L-P, Katz EJ, Gold MS (2010) BK_{Ca} currents are enriched in a subpopulation
669 of adult rat cutaneous nociceptive dorsal root ganglion neurons. Eur J Neurosci 31:450–462.

670 Zhang XF, Gopalakrishnan M, Shieh CC (2003) Modulation of action potential firing by
671 iberiotoxin and NS1619 in rat dorsal root ganglion neurons. Neuroscience 122:1003–1011.

672 Zheng Q, Fang D, Liu M, Cai J, Wan Y, Han J, Xing G (2013) Suppression of KCNQ/M (Kv7)
673 potassium channels in dorsal root ganglion neurons contributes to the development of bone

674 cancer pain in a rat model. Pain 154:434–448.

675
676
677
678
679
680
681
682
683
684
685
686
687
688
689
690
691
692
693
694
695
696
697
698
699
700
701
702
703
704
705

Figure Legends

Figure 1. Co-localization of the Kv3.4 channel with the peptidergic nociceptive marker calcitonin gene-related peptide (CGRP). Immunohistochemical staining demonstrating co-labeling of CGRP with Kv3.4 protein. Panels B and C are magnified areas of panel A.

Figure 2. Co-localization of the presynaptic Kv3.4 channel with the non-peptidergic nociceptive marker isolectin B4 (IB4). (**A**)-(**C**) Immunohistochemical staining demonstrating co-labeling of IB4 with Kv3.4 protein. Panels B and C are magnified areas of panel A. (**D**) Co-labeling of Kv3.4 protein with the glutamatergic presynaptic marker VGLUT2.

Figure 3. Intact cervical spinal cord preparation for patch-clamp recordings of glutamatergic synaptic currents from the superficial dorsal horn. (**A**) Schematic of the experimental set-up representing its main components. Neurons in the superficial dorsal horn are visualized using oblique infrared LED illumination and a 40x immersion objective. SC = spinal cord pinned at an angle of 10^{o} – 15^{o} on a piece of elastomer compound eraser. The spinal cord is represented by a cross section of the cervical region with its axis perpendicular to the plane of the image. BSE = bipolar stimulation electrode (suction electrode). DR = dorsal roots (one free and the other inside the suction electrode). PCE: patch-clamping electrode hooked up to a Multiclamp 700B amplifier. (**B**). Images of lamina I neurons subjected to whole-cell patch-clamping. *Top*, infrared image; *bottom*, fluorescence image of neuron loaded with biocytin (conjugated with Alexa Fluor 488) through the PCE. (**C**) Representative monosynaptic eEPSCs

evoked consecutively by stimulating the DR (100 μA, 1 ms, 10 sweeps) while holding the neuron's membrane potential (V_H) at -70 mV (Materials and Methods). The average trace is shown in black. (**D**) Histogram of eEPSC's peak amplitudes. The stimulus intensity ranged between 100 – 600 μA. (**E**) Consecutive eEPSCs recorded before and after exposing the spinal cord to 1 μM CNQX (averages are displayed in black and red, respectively). (**F**). Spontaneous glutamatergic synaptic currents at V_H = -70 mV before (black) and after (red) exposure to 1 μM CNQX.

Figure 4. Spiking examples from neurons in the superficial dorsal horn. (**A**) Subthreshold and suprathreshold responses evoked by a stimulus of 100 μA. (**B**) Pair of action potentials exhibiting an afterdepolarization. This response was evoked by a brief 0.5 ms stimulus. (**C**) Spontaneous spiking (RMP = -62 mV). (**D**) Recording of passive and active responses evoked by sustained current injection (-20 pA-30 pA). First active trace shown in red.

Figure 5. eEPSCs from superficial dorsal horn neurons are potentiated by submillimolar concentrations of TEA and 4-AP. (**A**) and (**B**) *Left* and *center*: Consecutive monosynaptic eEPSCs recorded before and after (15-20 sweeps) exposing the spinal cord to 50 μM 4-AP (A) and 500 μM TEA (B). Averages displayed in red. *Right*: pooled paired measurements of peak EPSCs before (control) and after exposure to 4-AP (A) and TEA (B) with box plots showing the percent change in peaks across paired experiments. Sample size and *p* values of the paired Student t-test are shown on the graphs. Stimulation parameters are as indicated in Fig. 2 legend and Materials and Methods. Each symbol in the graphs represents an independent response from a separate spinal cord (i.e., the sample size corresponds to number of animals examined). Percent

754 change box plots describe the data sets as follows: dashed and solid lines representing mean and
755 median, respectively; lower and upper edges of the box corresponding to 25 and 75 percentiles,
756 respectively; lower and upper whiskers corresponding to 5 and 95 percentiles, respectively; and
757 crosses representing minimum and maximum values.
758
759 **Figure 6. eEPSCs from superficial dorsal horn neurons are not affected by specific**
760 **inhibitors of Kv7, BK and Kv1 channels.** (**A**) – (**C**). *Left* and *center*: Consecutive
761 monosynaptic eEPSCs recorded before and after (2-30 sweeps) exposing the spinal cord to the
762 indicated K^+ channel inhibitors (XE991, IbTX, and α-DTX). Averages displayed in red. *Right*:
763 pooled paired measurements of peak EPSCs before (control) and after exposure to the indicated
764 inhibitors. Sample size and P values of the paired Student t-test are shown on the graphs.
765 Stimulation parameters are as indicated in Fig. 2 legend and Materials and Methods. Each
766 symbol in the graphs represents an independent response from a separate spinal cord (i.e., the
767 sample size corresponds to number of animals examined). Percent change box plots are
768 displayed to the right of summary data plots (Fig. 5 legend describes box plot characteristics).
769
770 **Figure 7. Determination of monosynaptic responses from individual eEPSC traces.**
771 Representative eEPSC traces from examples displayed in Fig. 5 demonstrating consistent
772 monosynaptic peaks across multiple traces (dashed red lines). The by-eye identification of the
773 peaks in individual traces was generally confirmed by determining the regions of the average
774 trace with the lowest variance around the average peak. The magnitude of these peaks was used
775 for the analysis of monosynaptic eEPSCs in Fig. 8.
776

Figure 8. Submillimolar 4-AP and TEA consistently potentiate monosynaptic EPSCs. Pooled paired average peaks from the multi-peak analysis (Fig. 7) before and after exposure to 50 μM 4-AP (**A**), 500 μM TEA (**B**), 100 nM IbTX (**C**), 30 μM XE991 (**D**), and 80 nM α-DTX (**E**). Color scheme displays the numerical order of peaks in a given recording (light grey = 1st peak, dark grey = 2nd peak, light blue = 3rd peak, dark blue = 4th peak, light pink = 5th peak, dark pink = 6th peak, averages shown in red). The *p* values of the paired Student t-test are shown on the graphs. Percent change box plots are displayed to the right of summary data plots (Fig. 5 legend describes box plot characteristics).

Figure 9. Submillimolar 4-AP and TEA decrease the paired pulse ratio (PPR). (**A**) and (**B**) Paired pulse (interstimulus interval = 30-80 ms) EPSC recordings before and after (10 sweeps) exposing the spinal cord to 50 μM 4-AP (A) and 500 μM TEA (B). *Right*: pooled paired measurements of the paired pulse ratio (PPR = P2/P1) before (control) and after exposure to 4-AP (A) and TEA (B). Sample size and *p* values of the paired Student t-test are shown on the graphs. All recordings were conducted at V_H = -70 mV. Stimulation parameters are as indicated in Fig. 2 legend and Materials and Methods. Each symbol in the graphs represents an independent response from a separate spinal cord (i.e., the sample size corresponds to number of animals examined).

Figure 10. Submillimolar TEA does not affect spontaneous EPSCs. (**A**) Representative sweeps of sEPSCs at -70 mV, before and after exposing the spinal cord to 500 μM TEA (*left* and *right*, respectively). Zoomed-in segments are also shown to demonstrate individual events. (**B**) Relative frequency histograms of peak EPSC amplitudes from three independent recordings

800 (three neurons each from three different spinal cords) before and after exposure to TEA. Relative
801 frequency is the fraction of sEPSCs that falls into a given bin (bin size = 0.75 pA). (**C**)
802 Cumulative plots of sEPSC amplitudes corresponding to the data shown in panel B. In all three
803 cases, the two-sample Kolmogorov-Smirnov test returned no difference between the control and
804 TEA plots. The *p* values are indicated on the plots.
805
806 **Figure 11. Analysis of the primary nociceptor action potentials in the absence and presence**
807 **of several K^+ channel inhibitors.** *Left* to *right*: Representative action potential traces, phase
808 plane plots, and changes in APD_{50}, APD_{90}, and maximum repolarization rate (derived from phase
809 plane plots) before and after exposure to 50 μM 4-AP (**A**), 500 μM TEA (**B**), 100 nM IbTX (**C**),
810 30 μM XE991 (**D**), and 80 nM α-DTX (**E**). Averages shown in black and *p* values of the paired
811 Student's t test are displayed on graphs. Additional properties are reported on Table 4.

Table 1. EPSC Properties

		n
Peak (pA)	272.39 ± 31.57	79
Rise Time (ms)	7.89 ± 0.65	79
Latency (ms)	21.19 ± 0.65	79
Jitter (ms)	1.63 ± 0.17	75

Peak calculated as the amplitude of the EPSC waveform.
Rise Time calculated as the time from 10% to 90% of the EPSC waveform.
Latency calculated as the time from the start of the stimulus to the peak amplitude.
Jitter calculated as the time variability in the start of the EPSC waveform across multiple traces.

Table 2. Passive and Active Properties of Second Order Dorsal Horn Neurons

		n
RMP (mV)	-74 ± 0.88	65
Input Resistance (GΩ)	0.95 ± 0.07	53
Capacitance (pF)	37.56 ± 3.84	37
Threshold (mV)	-55.65 ± 0.77	40
AP Amplitude (mV)	96.6 ± 1.81	40
ADP Amplitude (mV)	7.69 ± 0.7	24
AHP (mV)	-76.79 ± 1.21	16
APD_{50} (ms)	1.86 ± 0.09	40
APD_{90} (ms)	0.68 ± 0.03	40
Max depolarization rate (mV ms^{-1})	142.09 ± 8.29	40
Max repolarization rate (mV ms^{-1})	60.24 ± 4.01	40

RMP = Resting Membrane Potential; AP = Action Potential; ADP = Afterdepolarization; AHP = Afterhyperpolarization; APD_{50} = Action Potential Duration at 50% of the Amplitude; APD_{90} = Action Potential Duration at 90% of the Amplitude

AP Amplitude calculated as the difference from the most negative membrane potential to the most positive membrane potential during an AP waveform.
ADP Amplitude calculated from the most negative membrane potential to the peak of the ADP.
Max depolarization and repolarization rates determined from the derivative of the AP waveform.

Table 3. Effects of Pharmacological Compounds on EPSC Properties

	500 µM TEA		50 µM 4-AP		100 nM IbTX		30 µM XE991		80 nM DTX	
	Pre	Post	Pre	Post	Pre	Post	Pre	Post	Pre	Post
Peak (pA)	323.91 ± 121.32	370.27 ± 123.30*	193.91 ± 43.69	258.21 ± 49.75**	473.19 ± 178.68	502.68 ± 191.33	367.66 ± 85.29	322.93 ± 123.56	470.52 ± 203.08	461.1 ± 179.54
Rise Time (ms)	8.59 ± 1.60	9.81 ± 1.69	8.45 ± 2.00	7.96 ± 1.44	9.23 ± 3.27	8.48 ± 2.85	13.75 ± 3.17	13.05 ± 3.25	7.34 ± 2.23	7.35 ± 2.24
Latency (ms)	20.27 ± 2.34	20.45 ± 2.41	22.44 ± 3.06	22.77 ± 3.31	22.07 ± 4.15	21.63 ± 3.98	25.15 ± 4.32	25.99 ± 4.80	21.31 ± 5.71	21.60 ± 5.61
Jitter (ms)	1.66 ± 0.36	1.71 ± 0.31	2.07 ± 0.73	1.56 ± 0.45	1.8 ± 0.38	1.6 ± 0.52	2.83 ± 1.03	3.58 ± 1.29	1.38 ± 0.58	2.05 ± 0.80
n	9		7		8		5		4	

Peak is the maximum amplitude of the EPSC waveform.
Rise Time calculated as the time from 10% to 90% of the EPSC waveform.
Latency calculated as the time from the start of the stimulus to the peak amplitude.
Jitter calculated as the time variability in the start of the EPSC waveform across multiple traces.

* $p \leq 0.05$; ** $p \leq 0.01$

Table 4. Effects of Pharmacological Compounds on the DRG Action Potential

	500 μM TEA		50 μM 4-AP		100 nM IbTX		30 μM XE991		80 nM DTX	
	Pre	Post	Pre	Post	Pre	Post	Pre	Post	Pre	Post
Capacitance (pF)	12.88 ± 1.20		16.07 ± 4.52		13.83 ± 1.46		12.75 ± 1.47		12.73 ± 1.11	
Diameter (μm)	21.61 ± 0.93		20.78 ± 0.97		21.25 ± 1.02		21.43 ± 0.88		20.47 ± 0.97	
RMP (mV)	-62.36 ± 4.42	-65.50 ± 6.07	-67.25 ± 2.30	-71.50 ± 2.75*	-66.93 ± 2.90	-70.79 ± 3.67**	-66.07 ± 2.45	-64.93 ± 2.52	-64.88 ± 3.05	-69.88 ± 4.56
IR (GΩ)	0.55 ± 0.16	0.77 ± 0.19	1.06 ± 0.32	1.38 ± 0.33	0.76 ± 0.19	0.92 ± 0.23	0.93 ± 0.17	1.39 ± 0.29	0.89 ± 0.17	1.05 ± 0.15
Threshold (mV)	-29.21 ± 3.04	-32.64 ± 4.23	-28.63 ± 2.08	-31.88 ± 2.60*	-26.36 ± 3.82	-29.21 ± 4.31*	-29.07 ± 1.81	-30.36 ± 1.65	-29.88 ± 2.60	-35.00 ± 2.05*
Amplitude (mV)	113.05 ± 2.93	111.91 ± 4.63	115.47 ± 2.41	116.98 ± 3.86	108.08 ± 4.96	110.23 ± 6.26	109.97 ± 3.98	107.89 ± 3.24	110.79 ± 4.55	107.27 ± 5.39
AHP (mV)	-73.47 ± 2.35	-74.49 ± 5.45	-73.11 ± 1.54	-75.68 ± 2.14	-72.36 ± 2.24	-76.85 ± 3.01*	-73.32 ± 2.48	-73.35 ± 2.11	-71.63 ± 1.91	-76.34 ± 2.35
APD_{50} (ms)	4.33 ± 0.63	7.60 ± 1.27**	4.43 ± 0.47	6.28 ± 0.83*	4.15 ± 0.48	5.46 ± 0.90*	4.73 ± 0.53	5.16 ± 0.62	3.80 ± 0.43	3.67 ± 0.50
APD_{90} (ms)	1.04 ± 0.05	1.30 ± 0.06***	1.09 ± 0.07	1.40 ± 0.11*	1.05 ± 0.05	1.17 ± 0.10	1.13 ± 0.06	1.15 ± 0.07	1.05 ± 0.07	1.05 ± 0.09
Max depolarization Rate (mV/ms)	79.84 ± 17.67	79.35 ± 21.17	75.42 ± 8.83	69.75 ± 8.76	68.26 ± 10.93	67.01 ± 11.73	61.28 ± 8.94	55.55 ± 6.12	77.82 ± 12.72	71.50 ± 11.87
Max repolarization Rate (mV/ms)	38.37 ± 3.68	25.04 ± 2.30***	33.90 ± 2.64	25.94 ± 2.66*	37.99 ± 3.81	35.13 ± 4.95	35.38 ± 3.75	32.76 ± 2.91	38.04 ± 3.15	40.65 ± 4.17
n	7		8		7		7		8	

RMP = Resting membrane potential, AHP = Afterhyperpolarization, APD_{50} = Action potential duration at 50% of amplitude, APD_{90} = Action potential duration at 90% of amplitude * $p < 0.05$, ** $p \leq 0.01$, *** $p \leq 0.001$

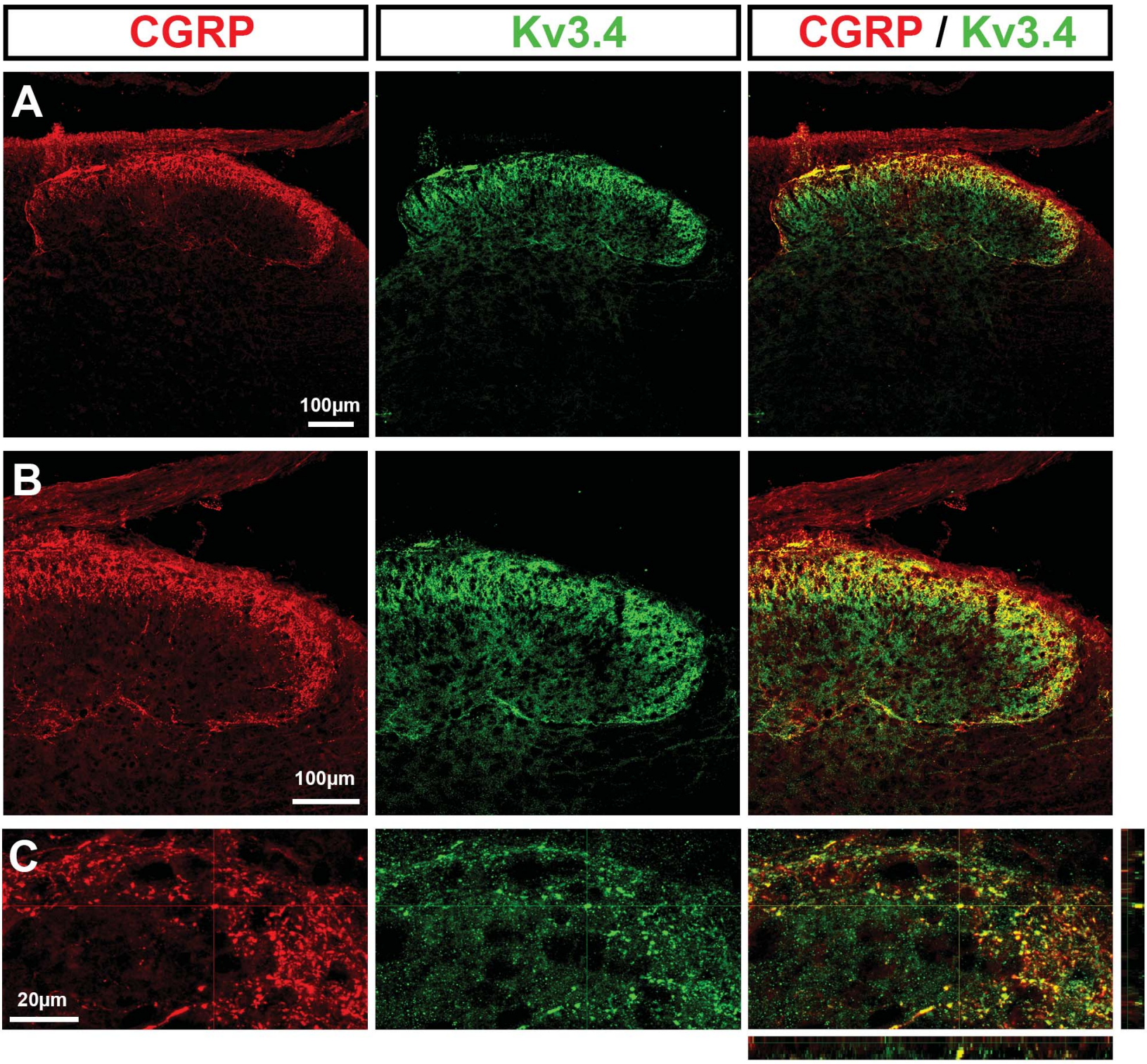
CGRP
Kv3.4
CGRP / Kv3.4
A
100μm
B
100μm
C
20μm

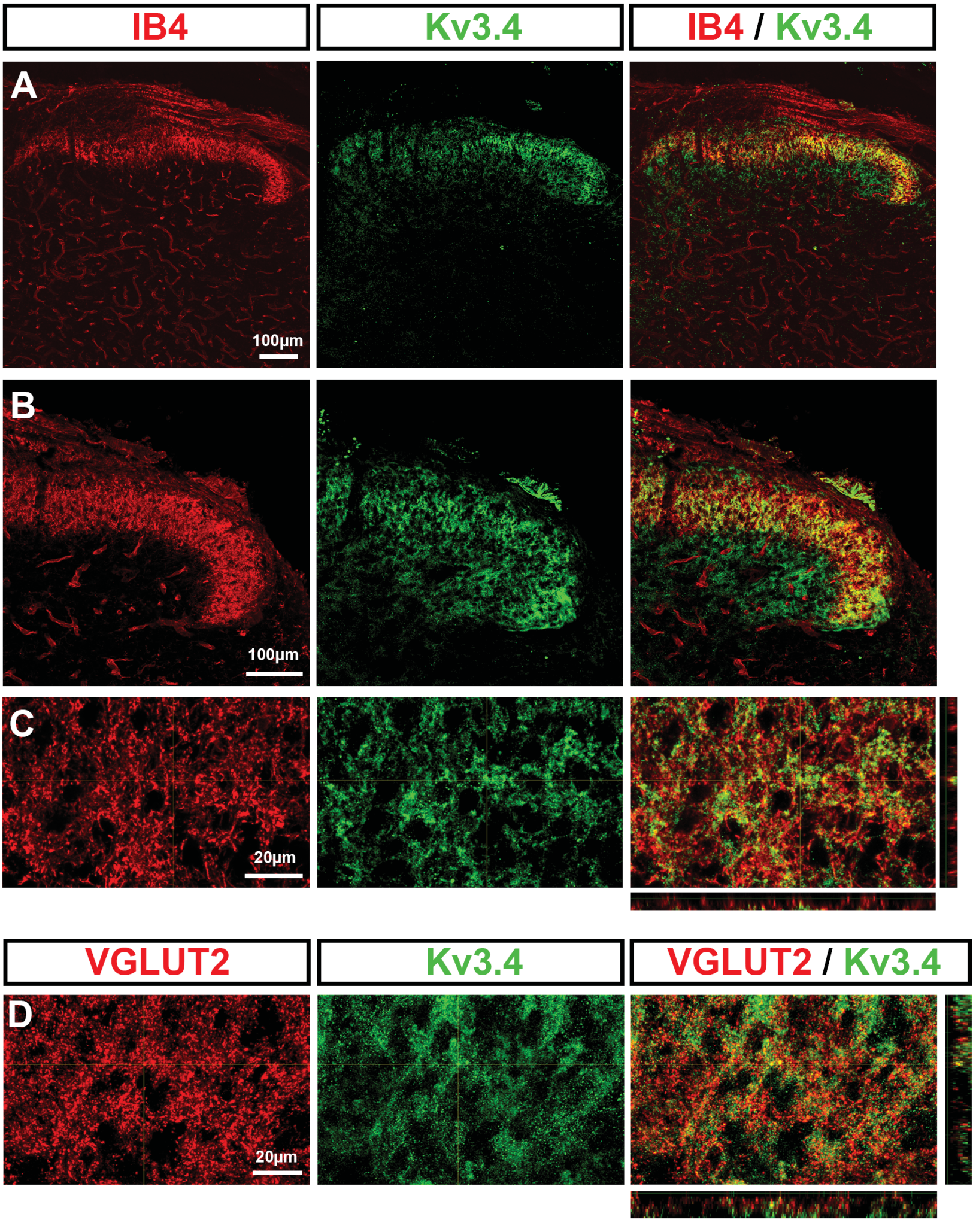
IB4
Kv3.4
IB4 / Kv3.4
A
100μm
B
100μm
C
20μm
VGLUT2
Kv3.4
VGLUT2 / Kv3.4
D
20μm

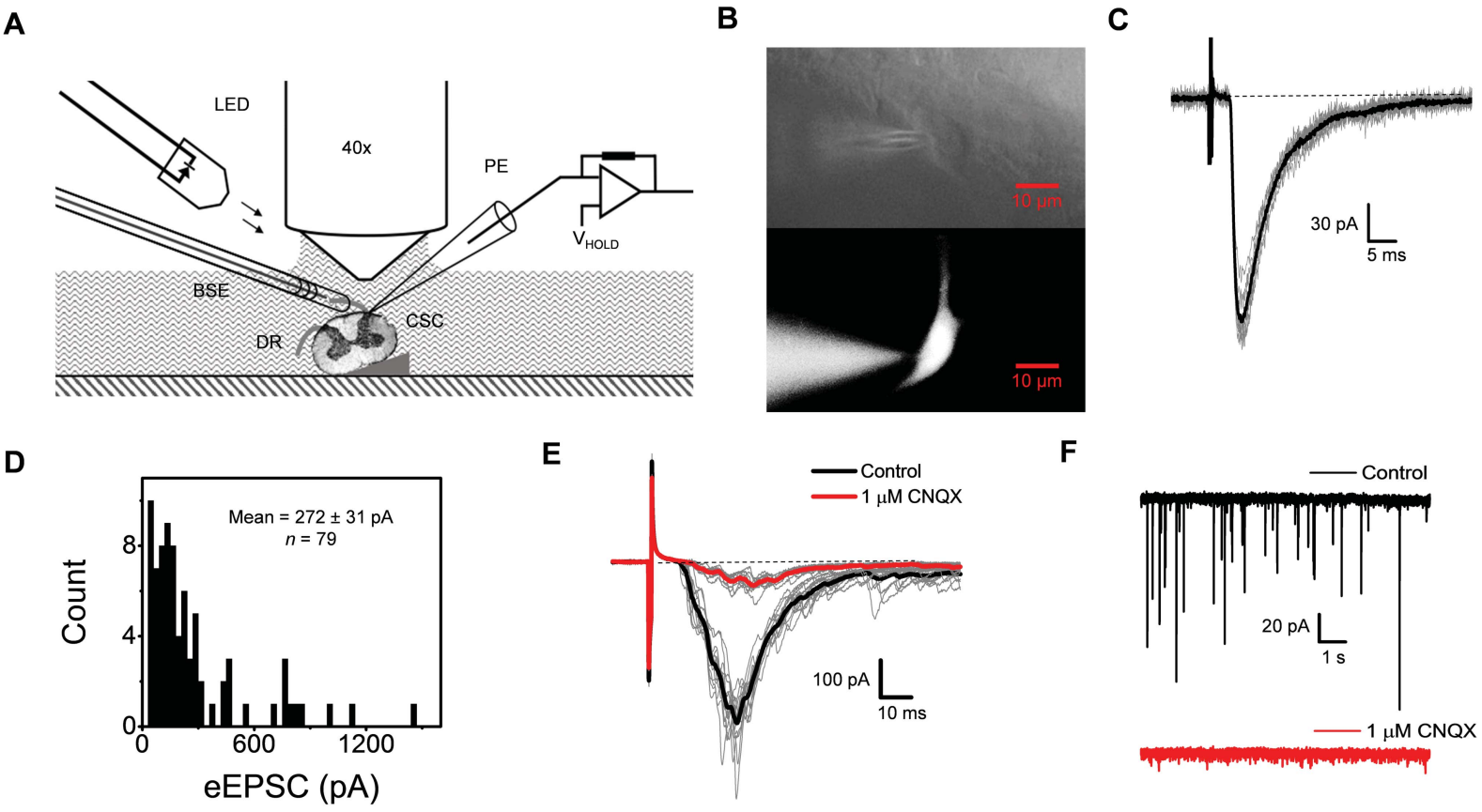
A
LED
40x
PE
V_{HOLD}
BSE
CSC
DR
B
10 µm
10 µm
C
30 pA
5 ms
D
Mean = 272 ± 31 pA
n = 79
Count
8
4
0
0
600
1200
eEPSC (pA)
E
Control
1 µM CNQX
100 pA
10 ms
F
Control
20 pA
1 s
1 µM CNQX

Figure 3

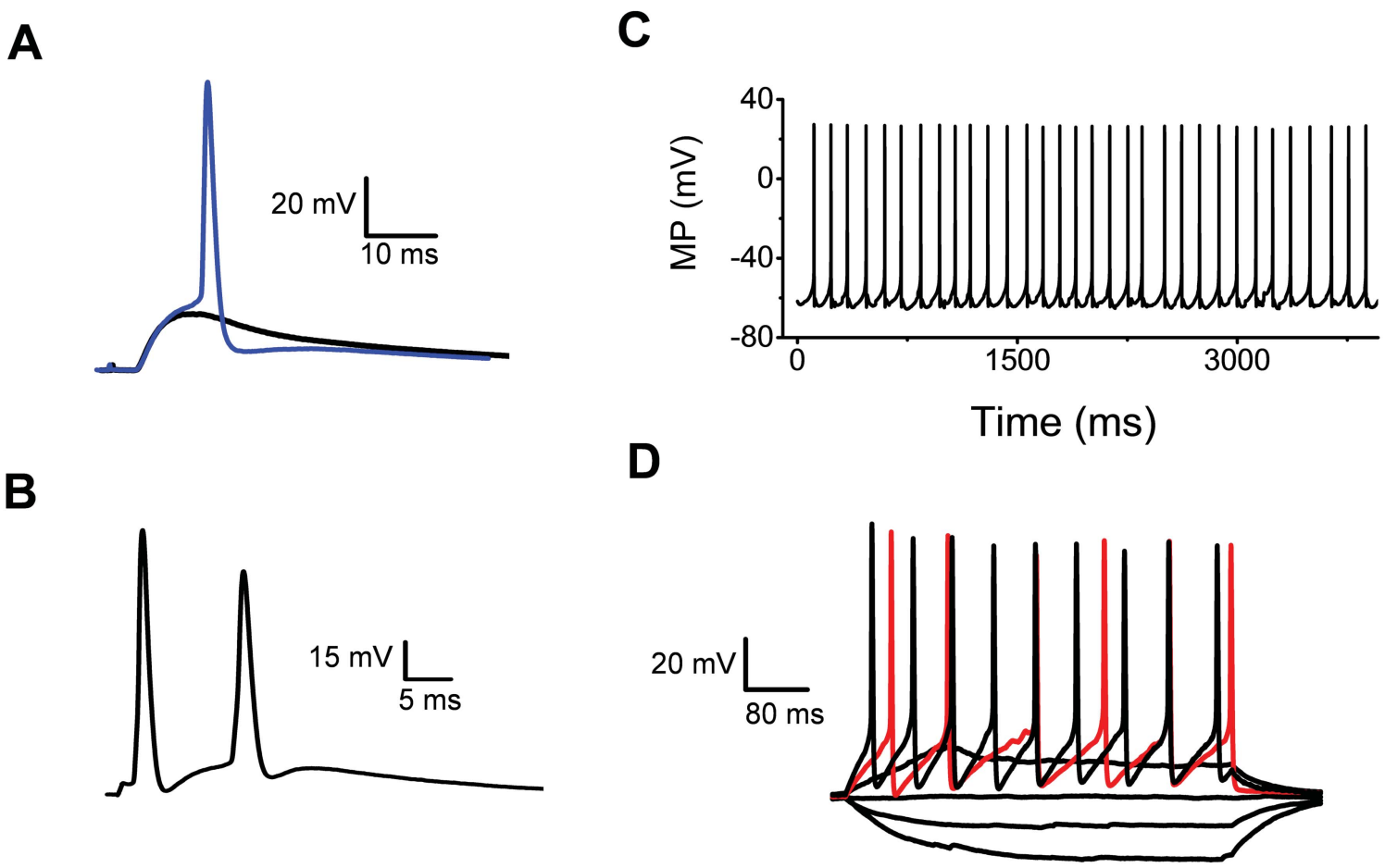
A
20 mV
10 ms
B
15 mV
5 ms
C
40
0
-40
-80
MP (mV)
0
1500
3000
Time (ms)
D
20 mV
80 ms

Figure 4

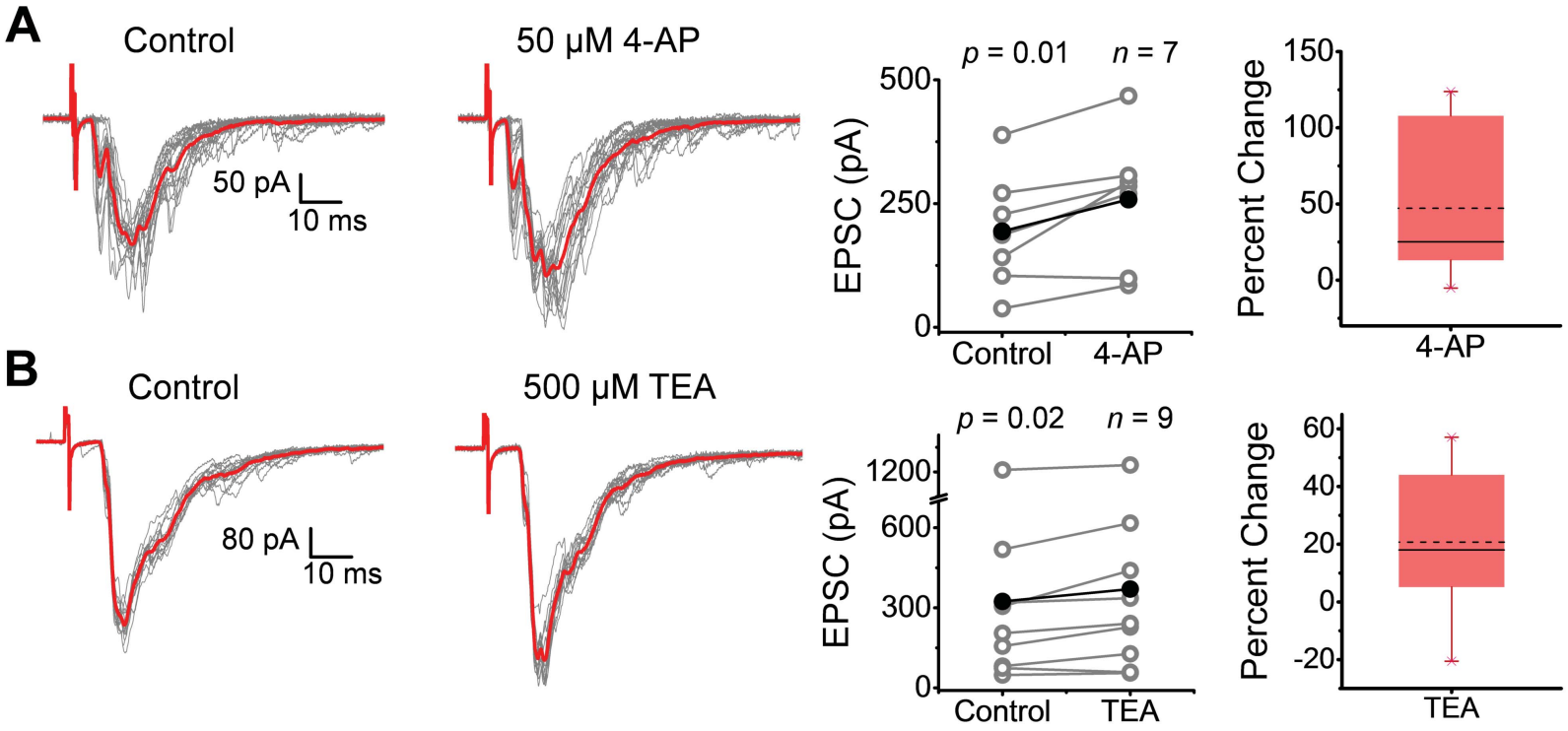
A
Control
50 µM 4-AP
50 pA
10 ms
p = 0.01
n = 7
EPSC (pA)
500
250
0
Control
4-AP
Percent Change
150
100
50
0
4-AP
B
Control
500 µM TEA
80 pA
10 ms
p = 0.02
n = 9
EPSC (pA)
1200
600
300
0
Control
TEA
Percent Change
60
40
20
0
-20
TEA

Figure 5

Figure 6

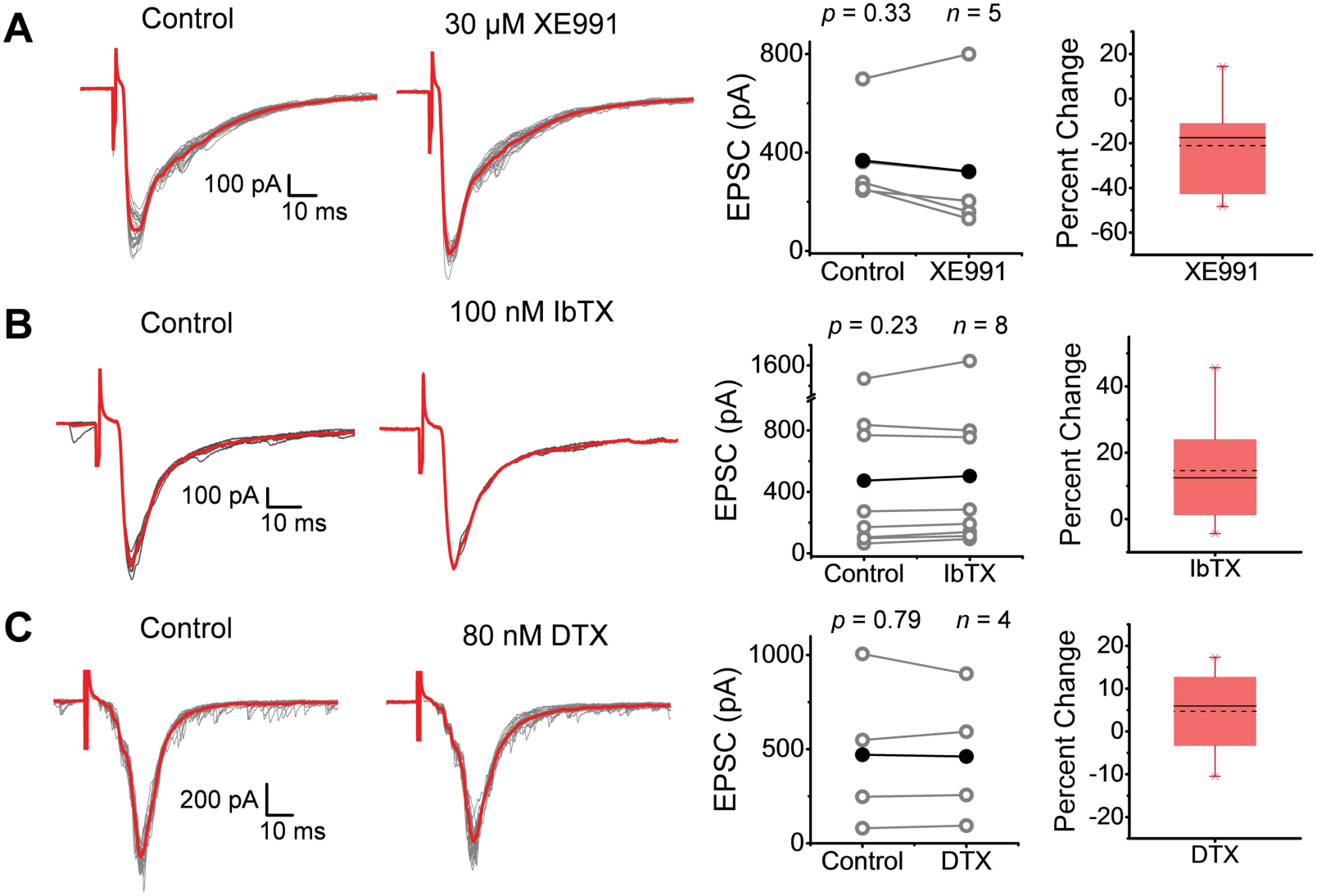
A
Control
30 μM XE991
100 pA
10 ms
p = 0.33
n = 5
EPSC (pA)
800
400
0
Control
XE991
Percent Change
20
0
-20
-40
-60
XE991
B
Control
100 nM IbTX
100 pA
10 ms
p = 0.23
n = 8
EPSC (pA)
1600
800
400
0
Control
IbTX
Percent Change
40
20
0
IbTX
C
Control
80 nM DTX
200 pA
10 ms
p = 0.79
n = 4
EPSC (pA)
1000
500
0
Control
DTX
Percent Change
20
10
0
-10
-20
DTX

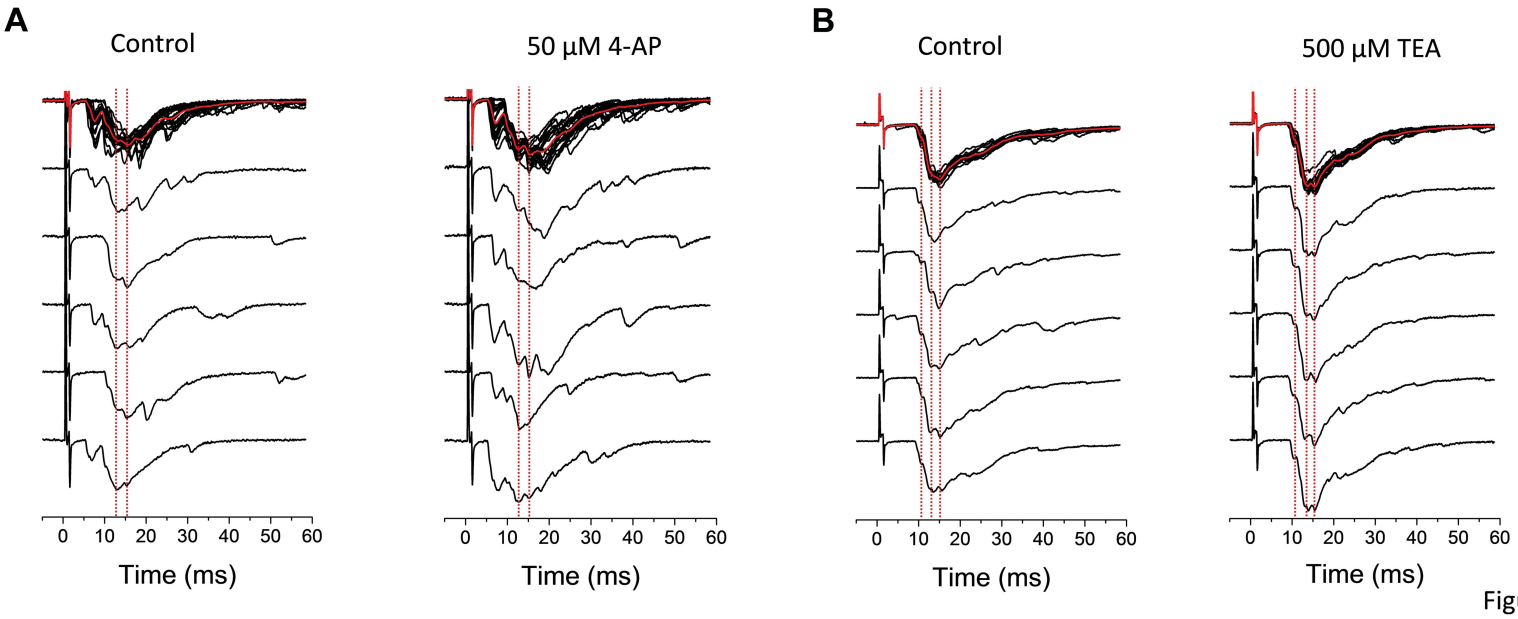
A
Control
50 µM 4-AP
B
Control
500 µM TEA
0 10 20 30 40 50 60
Time (ms)

Figure 7

Figure 8

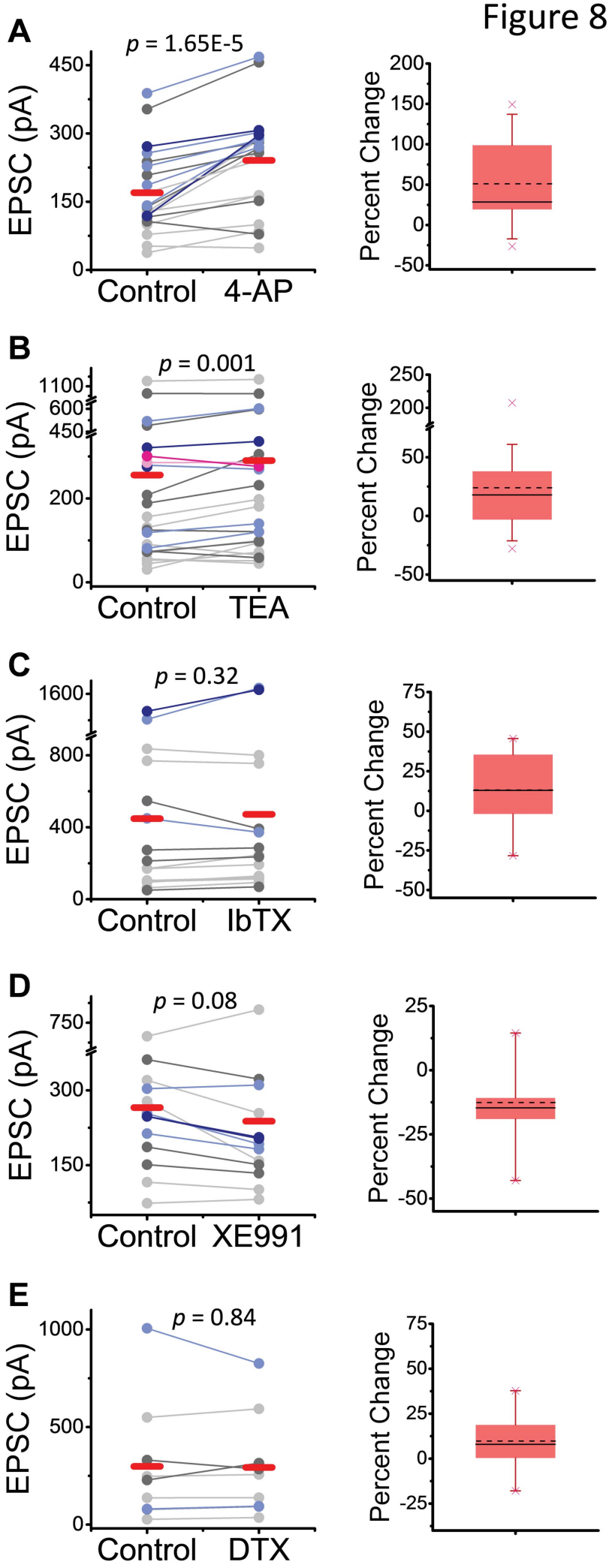
A
p = 1.65E-5
EPSC (pA)
450
300
150
0
Control
4-AP
Percent Change
200
150
100
50
0
-50
B
p = 0.001
EPSC (pA)
1100
600
450
200
0
Control
TEA
Percent Change
250
200
50
0
-50
C
p = 0.32
EPSC (pA)
1600
800
400
0
Control
IbTX
Percent Change
75
50
25
0
-25
-50
D
p = 0.08
EPSC (pA)
750
300
150
Control
XE991
Percent Change
25
0
-25
-50
E
p = 0.84
EPSC (pA)
1000
500
0
Control
DTX
Percent Change
75
50
25
0
-25

Figure 9

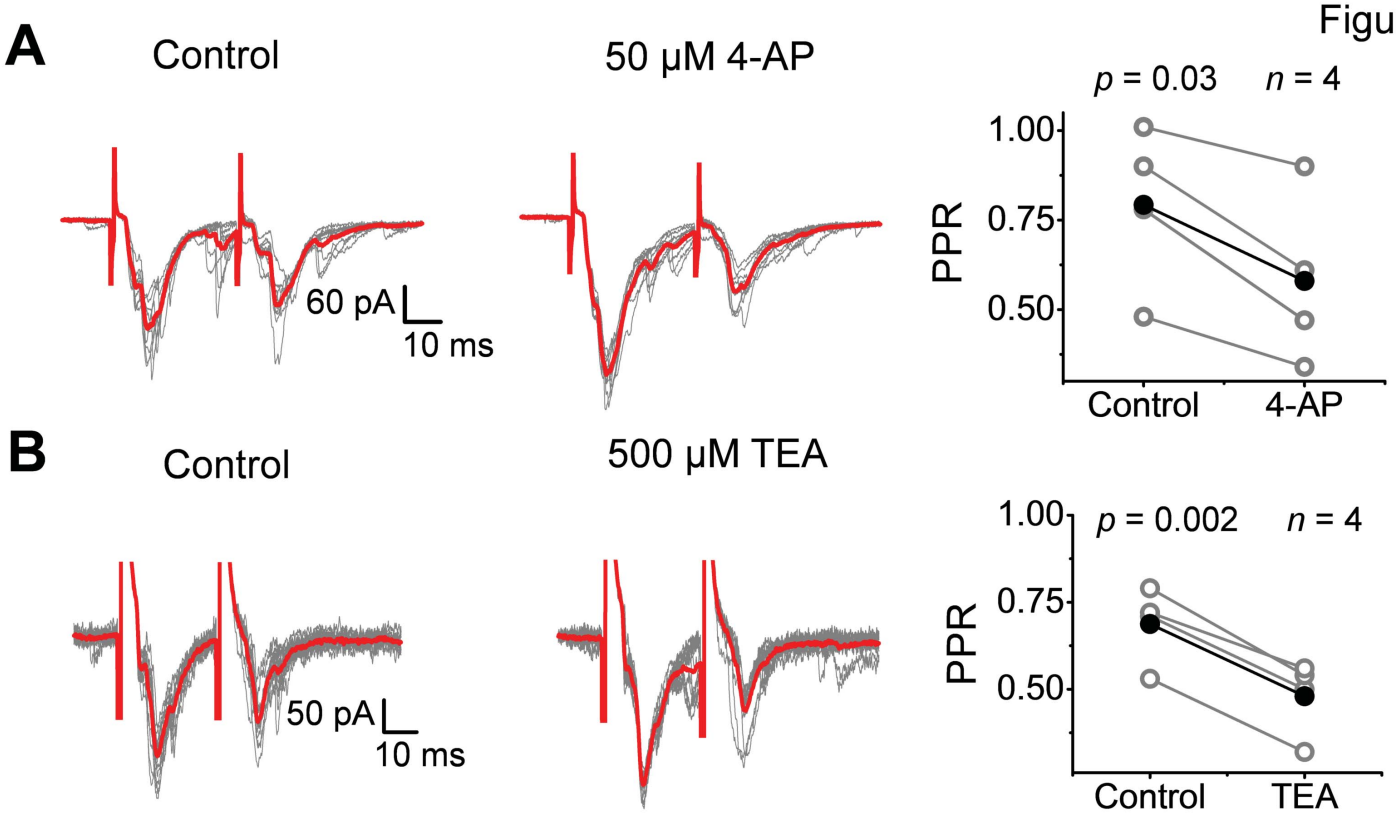
A
Control
50 μM 4-AP
60 pA
10 ms
p = 0.03
n = 4
1.00
0.75
0.50
PPR
Control
4-AP
B
Control
500 μM TEA
50 pA
10 ms
1.00
p = 0.002
n = 4
0.75
0.50
PPR
Control
TEA

Figure 10

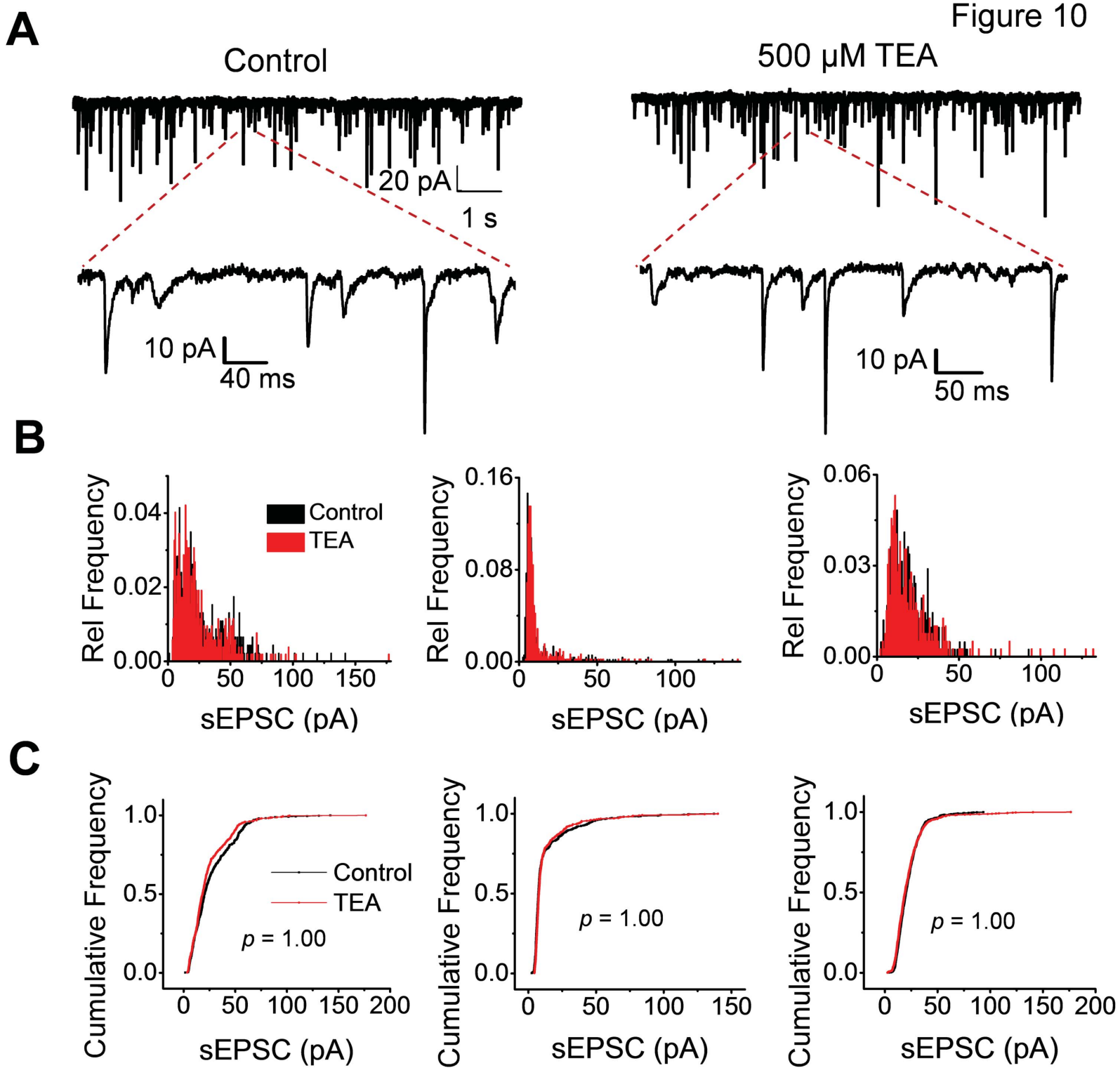
A
Control
500 μM TEA
20 pA
1 s
10 pA
40 ms
10 pA
50 ms
B
Rel Frequency
Control
TEA
sEPSC (pA)
C
Cumulative Frequency
Control
TEA
p = 1.00
sEPSC (pA)

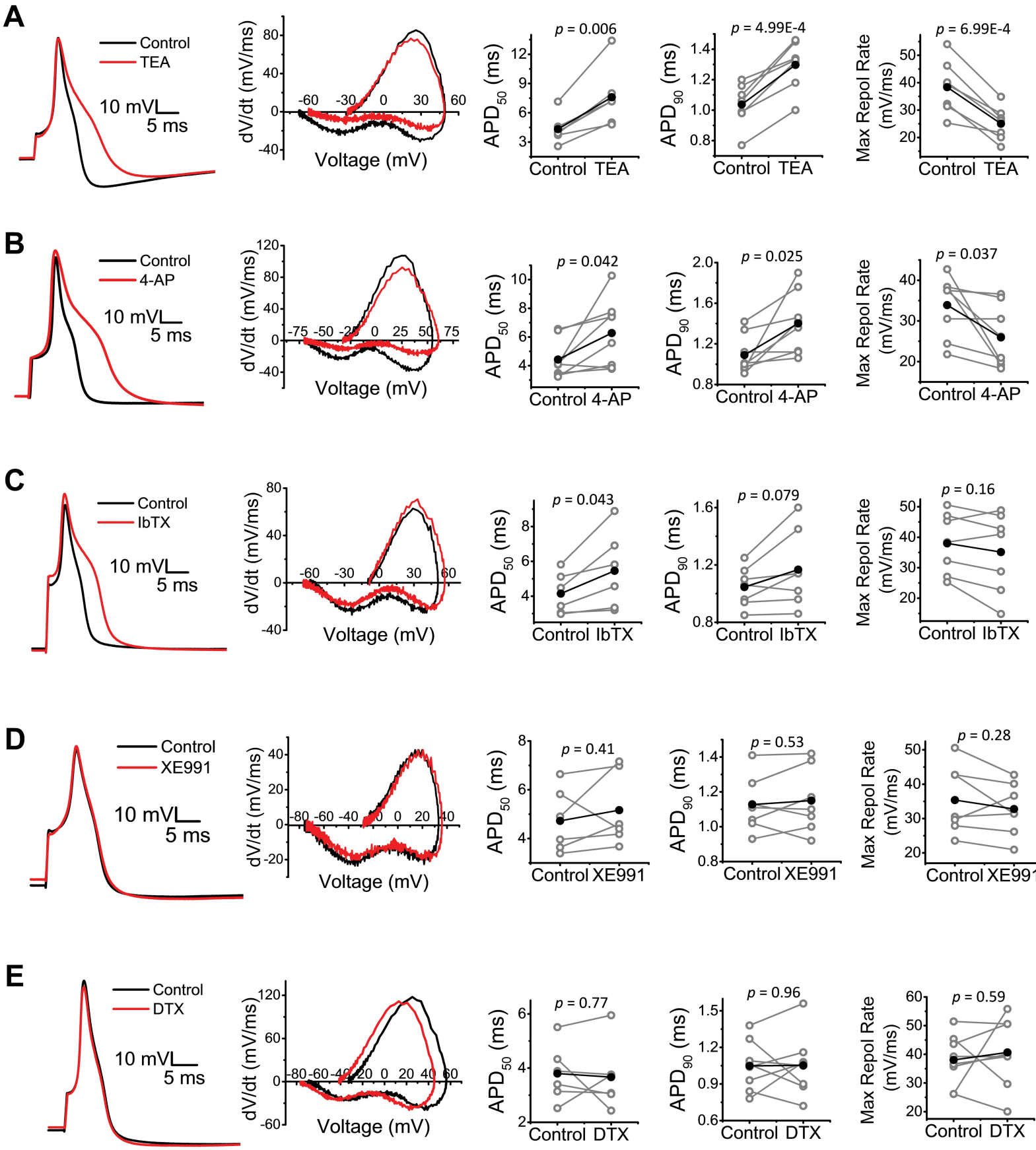
A
Control
TEA
10 mV
5 ms
dV/dt (mV/ms)
Voltage (mV)
p = 0.006
APD50 (ms)
Control TEA
p = 4.99E-4
APD90 (ms)
Control TEA
p = 6.99E-4
Max Repol Rate (mV/ms)
Control TEA
B
Control
4-AP
10 mV
5 ms
dV/dt (mV/ms)
Voltage (mV)
p = 0.042
APD50 (ms)
Control 4-AP
p = 0.025
APD90 (ms)
Control 4-AP
p = 0.037
Max Repol Rate (mV/ms)
Control 4-AP
C
Control
IbTX
10 mV
5 ms
dV/dt (mV/ms)
Voltage (mV)
p = 0.043
APD50 (ms)
Control IbTX
p = 0.079
APD90 (ms)
Control IbTX
p = 0.16
Max Repol Rate (mV/ms)
Control IbTX
D
Control
XE991
10 mV
5 ms
dV/dt (mV/ms)
Voltage (mV)
p = 0.41
APD50 (ms)
Control XE991
p = 0.53
APD90 (ms)
Control XE991
p = 0.28
Max Repol Rate (mV/ms)
Control XE991
E
Control
DTX
10 mV
5 ms
dV/dt (mV/ms)
Voltage (mV)
p = 0.77
APD50 (ms)
Control DTX
p = 0.96
APD90 (ms)
Control DTX
p = 0.59
Max Repol Rate (mV/ms)
Control DTX

Figure 11